ROS: A GNN-based Relax-Optimize-and-Sample Framework for Max-k-Cut Problems

Yeqing Qiu [1 2] Ye Xue [1 2] Akang Wang [1 2] Yiheng Wang [1 2] Qingjiang Shi [1 3] Zhi-Quan Luo [1 2]

Abstract

The Max-k-Cut problem is a fundamental combinatorial optimization challenge that generalizes the classic $\mathcal{NP}$-complete Max-Cut problem. While relaxation techniques are commonly employed to tackle Max-k-Cut, they often lack guarantees of equivalence between the solutions of the original problem and its relaxation. To address this issue, we introduce the Relax-Optimize-and-Sample (ROS) framework. In particular, we begin by relaxing the discrete constraints to the continuous probability simplex form. Next, we pre-train and fine-tune a graph neural network model to efficiently optimize the relaxed problem. Subsequently, we propose a sampling-based construction algorithm to map the continuous solution back to a high-quality Max-k-Cut solution. By integrating geometric landscape analysis with statistical theory, we establish the consistency of function values between the continuous solution and its mapped counterpart. Extensive experimental results on random regular graphs, the Gset benchmark, and the real-world datasets demonstrate that the proposed ROS framework effectively scales to large instances with up to $20,000$ nodes in just a few seconds, outperforming state-of-the-art algorithms. Furthermore, ROS exhibits strong generalization capabilities across both in-distribution and out-of-distribution instances, underscoring its effectiveness for large-scale optimization tasks.

1. Introduction

The *Max-k-Cut problem* involves partitioning the vertices of a graph into k disjoint subsets in such a way that the total weight of edges between vertices in different subsets is maximized. This problem represents a significant challenge in combinatorial optimization and finds applications across various fields, including telecommunication networks (Eisenblätter, 2002; Gui et al., 2019), data clustering (Poland & Zeugmann, 2006; Ly et al., 2023), and theoretical physics (Cook et al., 2019; Coja-Oghlan et al., 2022). The Max-k-Cut problem is known to be $\mathcal{NP}$-complete, as it generalizes the well-known *Max-Cut problem*, which is one of the 21 classic $\mathcal{NP}$-complete problems identified by Karp (1972).

Significant efforts have been made to develop methods for solving Max-k-Cut problems (Nath & Kuhnle, 2024). Ghaddar et al. (2011) introduced an exact branch-and-cut algorithm based on semi-definite programming, capable of handling graphs with up to 100 vertices. For larger instances, various polynomial-time approximation algorithms have been proposed. Goemans & Williamson (1995) addressed the Max-Cut problem by first solving a semi-definite relaxation to obtain a fractional solution, then applying a randomization technique to convert it into a feasible solution, resulting in a 0.878-approximation algorithm. Building on this, Frieze & Jerrum (1997) extended the approach to Max-k-Cut, offering feasible solutions with approximation guarantees. de Klerk et al. (2004) further improved these guarantees, while Shinde et al. (2021) optimized memory usage. Despite their strong theoretical performance, these approximation algorithms involve solving computationally intensive semi-definite programs, rendering them impractical for large-scale Max-k-Cut problems. A variety of heuristic methods have been developed to tackle the scalability challenge. For the Max-Cut problem, Burer et al. (2002) proposed rank-two relaxation-based heuristics, and Goudet et al. (2024) introduced a meta-heuristic approach using evolutionary algorithms. For Max-k-Cut, heuristics such as genetic algorithms (Li & Wang, 2016), greedy search (Gui et al., 2019), multiple operator heuristics (Ma & Hao, 2017), and local search (Garvardt et al., 2023) have been proposed. While these heuristics can handle much larger Max-k-Cut instances, they often struggle to balance efficiency and solution quality.

Recently, *machine learning* techniques have gained attention for enhancing optimization algorithms (Bengio et al.,

[1]Shenzhen Research Institute of Big Data, Shenzhen, China. [2]The Chinese University of Hong Kong, Shenzhen, China. [3]Tongji University, Shanghai, China. Correspondence to: Ye Xue <xueye@cuhk.edu.cn>.

Proceedings of the 42^{nd} International Conference on Machine Learning, Vancouver, Canada. PMLR 267, 2025.

2021; Gasse et al., 2022; Chen et al., 2024). Several studies, including Khalil et al. (2017); Barrett et al. (2020); Chen et al. (2020); Barrett et al. (2022), framed the Max-Cut problem as a sequential decision-making process, using reinforcement learning to train policy networks for generating feasible solutions. However, RL-based methods often suffer from extensive sampling efforts and increased complexity in action space when extended to Max-k-Cut, and hence entails significantly longer training and testing time. Karalias & Loukas (2020) focuses on subset selection, including Max-Cut as a special case. It trains a *graph neural network* (GNN) to produce a distribution over subsets of nodes of an input graph by minimizing a probabilistic penalty loss function. After the network has been trained, a randomized algorithm is employed to sequentially decode a valid Max-Cut solution from the learned distribution. A notable advancement by Schuetz et al. (2022) reformulated Max-Cut as a quadratic unconstrained binary optimization (QUBO), removing binarity constraints to create a differentiable loss function. This loss function was used to train a GNN, followed by a simple projection onto integer variables after unsupervised training. The key feature of this approach is solving the Max-Cut problem during the training phase, eliminating the need for a separate testing stage. Although this method can produce high-quality solutions for Max-Cut instances with millions of nodes, the computational time remains significant due to the need to optimize a parameterized GNN from scratch. The work of Tönshoff et al. (2023) first formulated the Max-Cut problem as a *Constraint Satisfaction Problem* (CSP) and then proposed a novel GNN-based reinforcement learning approach. This method outperforms prior neural combinatorial optimization techniques and conventional search heuristics. However, to the best of our knowledge, it is limited to unweighted Max-k-Cut problems. NeuroCUT (Shah et al., 2024) is a partitioning method based on reinforcement learning, whereas DGCLUSTER (Bhowmick et al., 2024) and DMoN (Tsitsulin et al., 2023) utilize GNNs to optimize clustering objectives. However, these methods are specifically designed for graph clustering, which focuses on minimizing inter-cluster connections—contrary to Max-k-Cut, where the goal is to maximize inter-partition connections. Consequently, they are not directly applicable to our problem. Although NeuroCUT claims support for arbitrary objective functions, its node selection heuristics are tailored exclusively for graph clustering, rendering it unsuitable for Max-k-Cut.

In this work, we propose a GNN-based *Relax-Optimize-and-Sample* (ROS) framework for efficiently solving the Max-k-Cut problem with arbitrary edge weights. The framework is depicted in Figure 1. Initially, the Max-k-Cut problem is formulated as a discrete optimization task. To handle this, we introduce *probability simplex relaxations*, transforming the discrete problem into a continuous one. We then optimize the relaxed formulation by training parameterized GNNs in an unsupervised manner. To further improve efficiency, we apply *transfer learning*, utilizing pre-trained GNNs to warm-start the training process. Finally, we refine the continuous solution using a *random sampling algorithm*, resulting in high-quality Max-k-Cut solutions.

The key contributions of our work are summarized as follows:

- **Novel Framework.** We propose a scalable ROS framework tailored to the weighted Max-k-Cut problem with arbitrary signs, built on solving continuous relaxations using efficient learning-based techniques.
- **Theoretical Foundations.** We conduct a rigorous theoretical analysis of both the relaxation and sampling steps. By integrating geometric landscape analysis with statistical theory, we demonstrate the consistency of function values between the continuous solution and its sampled discrete counterpart.
- **Superior Performance.** Comprehensive experiments on public benchmark datasets show that our framework produces high-quality solutions for Max-k-Cut instances with up to $20,000$ nodes in just a few seconds. Our approach significantly outperforms state-of-the-art algorithms, while also demonstrating strong generalization across various instance types.

2. Preliminaries

2.1. Max-k-Cut Problems

Let $\mathcal{G} = (\mathcal{V}, \mathcal{E})$ represent an undirected graph with vertex set $\mathcal{V}$ and edge set $\mathcal{E}$. Each edge $(i, j) \in \mathcal{E}$ is assigned an arbitrary weight $\boldsymbol{W}_{ij} \in \mathbb{R}$, which can have any sign. A *cut* in $\mathcal{G}$ refers to a partition of its vertex set. The Max-k-Cut problem involves finding a k-partition $(\mathcal{V}_1, \ldots, \mathcal{V}_k)$ of the vertex set $\mathcal{V}$ such that the sum of the weights of the edges between different partitions is maximized.

To represent this partitioning, we employ a k-dimensional one-hot encoding scheme. Specifically, we define a $k \times N$ matrix $\boldsymbol{X} \in \mathbb{R}^{k\times N}$ where each column represents a one-hot vector. The Max-k-Cut problem can be formulated as:

$$\begin{aligned} \max_{\boldsymbol{X}\in\mathbb{R}^{k\times N}} \quad & \frac{1}{2}\sum_{i=1}^{N}\sum_{j=1}^{N}\boldsymbol{W}_{ij}\left(1-\boldsymbol{X}_{\cdot i}^{\top}\boldsymbol{X}_{\cdot j}\right) \\ \text{s. t.} \quad & \boldsymbol{X}_{\cdot j}\in\{\boldsymbol{e}_1, \boldsymbol{e}_2, \ldots, \boldsymbol{e}_k\} \qquad \forall j \in \mathcal{V}, \end{aligned} \tag{1}$$

where $\boldsymbol{X}_{\cdot j}$ denotes the j^{th} column of $\boldsymbol{X}$, $\boldsymbol{W}$ is a symmetric matrix with zero diagonal entries, and $\boldsymbol{e}_\ell \in \mathbb{R}^k$ is a one-hot vector with the ℓ^{th} entry set to 1. This formulation aims to maximize the total weight of edges between different partitions, ensuring that each node is assigned to exactly one

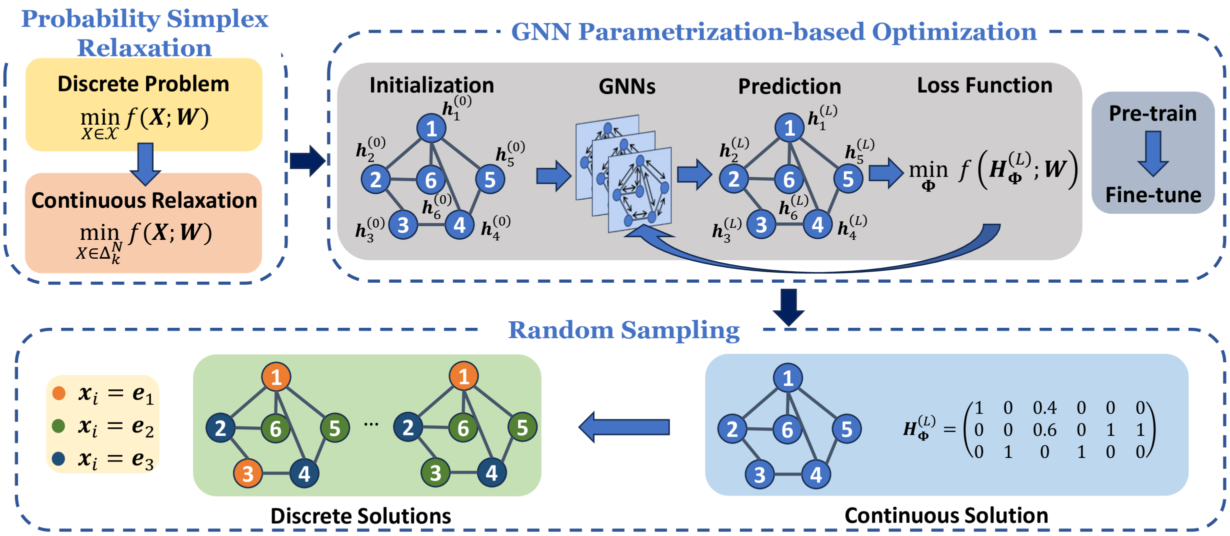

Figure 1: The Relax-Optimize-and-Sample framework.

partition, represented by the one-hot encoded vectors. We remark that weighted Max-k-Cut problems with arbitrary signs is a generalization of classic Max-Cut problems and arise in many interesting applications (De Simone et al., 1995; Poland & Zeugmann, 2006; Hojny et al., 2021).

2.2. Graph Neural Networks

GNNs are powerful tools for learning representations from graph-structured data. GNNs operate by iteratively aggregating information from a node's neighbors, enabling each node to capture increasingly larger sub-graph structures as more layers are stacked. This process allows GNNs to learn complex patterns and relationships between nodes, based on their local connectivity.

At the initial layer ($l = 0$), each node $i \in \mathcal{V}$ is assigned a feature vector $\boldsymbol{h}_i^{(0)}$, which typically originates from node features or labels. The representation of node i is then recursively updated at each subsequent layer through a parametric aggregation function $f_{\boldsymbol{\Phi}^{(l)}}$, defined as:

$$\boldsymbol{h}_i^{(l)} = f_{\boldsymbol{\Phi}^{(l)}}\left(\boldsymbol{h}_i^{(l-1)}, \{\boldsymbol{h}_j^{(l-1)} : j \in \mathcal{N}(i)\}\right), \quad (2)$$

where $\boldsymbol{\Phi}^{(l)}$ represents the trainable parameters at layer l, $\mathcal{N}(i)$ denotes the set of neighbors of node i, and $\boldsymbol{h}_i^{(l)}$ is the node's embedding at layer l for $l \in \{1, 2, \cdots, L\}$. This iterative process enables the GNN to propagate information throughout the graph, capturing both local and global structural properties.

3. A Relax-Optimize-and-Sample Framework

In this work, we leverage continuous optimization techniques to tackle Max-k-Cut problems, introducing a novel ROS framework. Acknowledging the inherent challenges of discrete optimization, we begin by relaxing the problem to probability simplices and concentrate on optimizing this relaxed version. To achieve this, we propose a machine learning-based approach. Specifically, we model the relaxed problem using GNNs, pre-training the GNN on a curated graph dataset before fine-tuning it on the specific target instance. After obtaining high-quality solutions to the relaxed continuous problem, we employ a random sampling procedure to derive a discrete solution that preserves the same objective value.

3.1. Probability Simplex Relaxations

To simplify the formulation of the problem (1), we remove constant terms and negate the objective function, yielding an equivalent formulation expressed as follows:

$$\min_{\boldsymbol{X} \in \mathcal{X}} \quad f(\boldsymbol{X}; \boldsymbol{W}) \coloneqq \mathrm{Tr}(\boldsymbol{X}\boldsymbol{W}\boldsymbol{X}^\top), \quad (\mathbf{P})$$

where $\mathcal{X} \coloneqq \left\{\boldsymbol{X} \in \mathbb{R}^{k \times N} : \boldsymbol{X}_{\cdot j} \in \{\boldsymbol{e}_1, \boldsymbol{e}_2, \ldots, \boldsymbol{e}_k\}, \forall j \in \mathcal{V}\right\}$. It is important to note that the matrix $\boldsymbol{W}$ is indefinite due to its diagonal entries being set to zero.

Given the challenges associated with solving the discrete problem $\mathbf{P}$, we adopt a naive relaxation approach, obtaining the convex hull of $\mathcal{X}$ as the Cartesian product of N k-dimensional probability simplices, denoted by Δ_k^N. Consequently, the discrete problem $\mathbf{P}$ is relaxed into the following continuous optimization form:

$$\min_{\boldsymbol{X} \in \Delta_k^N} \quad f(\boldsymbol{X}; \boldsymbol{W}). \qquad (\overline{\mathbf{P}})$$

Before optimizing problem $\overline{\mathbf{P}}$, we will characterize its *geometric landscape*. To facilitate this, we introduce the following definition.

Definition 3.1. Let $\overline{\boldsymbol{X}}$ denote a point in Δ_k^N. We define the neighborhood induced by $\overline{\boldsymbol{X}}$ as follows:

$$\mathcal{N}(\overline{\boldsymbol{X}}) := \left\{ \boldsymbol{X} \in \Delta_k^N \;\middle|\; \sum_{i \in \mathcal{K}(\overline{\boldsymbol{X}}_{\cdot j})} \boldsymbol{X}_{ij} = 1, \quad \forall j \in \mathcal{V} \right\},$$

where $\mathcal{K}(\overline{\boldsymbol{X}}_{\cdot j}) := \{i \in \{1, \ldots, k\} \mid \overline{\boldsymbol{X}}_{ij} > 0\}$.

The set $\mathcal{N}(\overline{\boldsymbol{X}})$ represents a neighborhood around $\overline{\boldsymbol{X}}$, where each point in $\mathcal{N}(\overline{\boldsymbol{X}})$ can be derived by allowing each non-zero entry of the matrix $\overline{\boldsymbol{X}}$ to vary freely, while the other entries are set to zero. Utilizing this definition, we can establish the following theorem.

Theorem 3.2. *Let $\boldsymbol{X}^\star$ denote a globally optimal solution to $\overline{\boldsymbol{P}}$, and let $\mathcal{N}(\boldsymbol{X}^\star)$ be its induced neighborhood. Then*

$$f(\boldsymbol{X}; \boldsymbol{W}) = f(\boldsymbol{X}^\star; \boldsymbol{W}), \quad \forall \boldsymbol{X} \in \mathcal{N}(\boldsymbol{X}^\star).$$

Theorem 3.2 states that for a globally optimal solution $\boldsymbol{X}^\star$, every point within its neighborhood $\mathcal{N}(\boldsymbol{X}^\star)$ shares the same objective value as $\boldsymbol{X}^\star$, thus forming a *basin* in the geometric landscape of $f(\boldsymbol{X}; \boldsymbol{W})$. If $\boldsymbol{X}^\star \in \mathcal{X}$ (i.e., an integer solution), then $\mathcal{N}(\boldsymbol{X}^\star)$ reduces to the singleton set $\{\boldsymbol{X}^\star\}$. Conversely, if $\boldsymbol{X}^\star \notin \mathcal{X}$, there exist $\prod_{j \in \mathcal{V}} |\mathcal{K}(\boldsymbol{X}^\star_{\cdot j})|$ unique integer solutions within $\mathcal{N}(\boldsymbol{X}^\star)$ that maintain the same objective value as $\boldsymbol{X}^\star$. This indicates that once a globally optimal solution to the relaxed problem $\overline{\mathbf{P}}$ is identified, it becomes straightforward to construct an optimal solution for the original problem $\mathbf{P}$ that preserves the same objective value.

According to Carlson & Nemhauser (1966), among all globally optimal solutions to the relaxed problem $\overline{\mathbf{P}}$, the integer solution always exists. Theorem 3.2 extends this result, indicating that if the globally optimal solution is fractional, we can provide a straightforward method to derive its integer counterpart. We remark that it is highly non-trivial to guarantee that the feasible Max-k-Cut solution obtained from the relaxation one has the same quality.

Example. Consider a Max-Cut problem ($k = 2$) associated with the weight matrix $\boldsymbol{W}$. We optimize its relaxation and obtain the optimal solution $\boldsymbol{X}^\star$.

$$\boldsymbol{W} := \begin{pmatrix} 0 & 1 & 1 \\ 1 & 0 & 1 \\ 1 & 1 & 0 \end{pmatrix}, \boldsymbol{X}^\star := \begin{pmatrix} p & 1 & 0 \\ 1-p & 0 & 1 \end{pmatrix},$$

where $p \in [0, 1]$. From the neighborhood $\mathcal{N}(\boldsymbol{X}^\star)$, we can identify the following integer solutions that maintain the same objective value.

$$\boldsymbol{X}_1^\star = \begin{pmatrix} 0 & 1 & 0 \\ 1 & 0 & 1 \end{pmatrix}, \boldsymbol{X}_2^\star = \begin{pmatrix} 1 & 1 & 0 \\ 0 & 0 & 1 \end{pmatrix}.$$

Given that $\overline{\mathbf{P}}$ is a non-convex program, identifying its global minimum is challenging. Consequently, the following two critical questions arise.

Q1. Since solving $\overline{\mathbf{P}}$ to global optimality is $\mathcal{NP}$-hard, how to efficiently optimize $\overline{\mathbf{P}}$ for high-quality solutions?

Q2. Given $\overline{\boldsymbol{X}} \in \Delta_k^N \setminus \mathcal{X}$ as a high-quality solution to $\overline{\mathbf{P}}$, can we construct a feasible solution $\hat{\boldsymbol{X}} \in \mathcal{X}$ to $\mathbf{P}$ such that $f(\hat{\boldsymbol{X}}; \boldsymbol{W}) = f(\overline{\boldsymbol{X}}; \boldsymbol{W})$?

We provide a positive answer to **Q2** in Section 3.2, while our approach to addressing **Q1** is deferred to Section 3.3.

3.2. Random Sampling

Let $\overline{\boldsymbol{X}} \in \Delta_k^N \setminus \mathcal{X}$ be a feasible solution to the relaxation $\overline{\mathbf{P}}$. Our goal is to construct a feasible solution $\boldsymbol{X} \in \mathcal{X}$ for the original problem $\mathbf{P}$, ensuring that the corresponding objective values are equal. Inspired by Theorem 3.2, we propose a *random sampling* procedure, outlined in Algorithm 1. In this approach, we sample each column $\boldsymbol{X}_{\cdot i}$ of the matrix $\boldsymbol{X}$ from a categorical distribution characterized by the event probabilities $\overline{\boldsymbol{X}}_{\cdot i}$ (denoted as Cat$(\boldsymbol{x}; \boldsymbol{p} = \overline{\boldsymbol{X}}_{\cdot i})$ in Step 3 of Algorithm 1). This randomized approach yields a feasible solution $\hat{\boldsymbol{X}}$ for $\mathbf{P}$. However, since Algorithm 1 incorporates randomness in generating $\hat{\boldsymbol{X}}$ from $\overline{\boldsymbol{X}}$, the value of $f(\hat{\boldsymbol{X}}; \boldsymbol{W})$ becomes random as well. This raises the critical question: is this value greater or lesser than $f(\overline{\boldsymbol{X}}; \boldsymbol{W})$? We address this question in Theorem 3.3.

Algorithm 1 Random Sampling

1: **Input:** $\overline{\boldsymbol{X}} \in \Delta_k^N$
2: **for** $i = 1$ to N **do**
3: $\quad \hat{\boldsymbol{X}}_{\cdot i} \sim$ Cat$(\boldsymbol{x}; \boldsymbol{p} = \overline{\boldsymbol{X}}_{\cdot i})$
4: **end for**
5: **Output:** $\hat{\boldsymbol{X}} \in \mathcal{X}$

Theorem 3.3. *Let $\overline{\boldsymbol{X}}$ and $\hat{\boldsymbol{X}}$ denote the input and output of Algorithm 1, respectively. Then, we have $\mathbb{E}_{\hat{\boldsymbol{X}}}[f(\hat{\boldsymbol{X}}; \boldsymbol{W})] = f(\overline{\boldsymbol{X}}; \boldsymbol{W})$.*

Theorem 3.3 states that $f(\hat{\boldsymbol{X}}; \boldsymbol{W})$ is equal to $f(\overline{\boldsymbol{X}}; \boldsymbol{W})$ in expectation. This implies that the random sampling procedure operates on a fractional solution, yielding Max-k-Cut feasible solutions with the same objective values in a probabilistic sense. While the Lovász-extension-based method (Bach, 2013) also offers a framework for continuous relaxation, achieving similar theoretical results for arbitrary k and edge weights $\boldsymbol{W}_{i,j} \in \mathbb{R}$ is not always guaranteed. In practice, we execute Algorithm 1 T times and select the solution with the lowest objective value of f as our best result. We remark that the theoretical interpretation in Theorem 3.3 distinguishes our sampling algorithm from the existing ones in the literature (Karalias & Loukas, 2020; Tönshoff et al., 2021; Michael et al., 2024).

3.3. GNN Parametrization-Based Optimization

To solve the problem $\overline{\mathbf{P}}$, we propose an efficient learning-to-optimize (L2O) method based on GNN parametrization. This approach reduces the laborious iterations typically required by classical optimization methods (e.g., mirror descent). Additionally, we introduce a “pre-train + fine-tune” strategy, where the model is endowed with prior graph knowledge during the pre-training phase, significantly decreasing the computational time required to optimize $\overline{\mathbf{P}}$.

GNN Parametrization. The Max-k-Cut problem can be framed as a node classification task, allowing us to leverage GNNs to aggregate node features, and obtain high-quality solutions. Initially, we assign a random embedding $\boldsymbol{h}_i^{(0)}$ to each node i in the graph $\mathcal{G}$. We adopt the GNN architecture proposed by Morris et al. (2019), utilizing an L-layer GNN with updates at layer l given by:

$$\boldsymbol{h}_i^{(l)} := \sigma\left(\boldsymbol{\Phi}_1^{(l)}\boldsymbol{h}_i^{(l-1)} + \boldsymbol{\Phi}_2^{(l)}\sum_{j\in\mathcal{N}(i)}\boldsymbol{W}_{ji}\boldsymbol{h}_j^{(l-1)}\right),$$

where $\sigma(\cdot)$ is an activation function, and $\boldsymbol{\Phi}_1^{(l)}$ and $\boldsymbol{\Phi}_2^{(l)}$ are the trainable parameters at layer l. This formulation facilitates efficient learning of node representations by leveraging both node features and the underlying graph structure. After processing through L layers of GNN, we obtain the final output $\boldsymbol{H}_{\boldsymbol{\Phi}}^{(L)} := [\boldsymbol{h}_1^{(L)}, \ldots, \boldsymbol{h}_N^{(L)}] \in \mathbb{R}^{k\times N}$. A softmax activation function is applied in the last layer to ensure $\boldsymbol{H}_{\boldsymbol{\Phi}}^{(L)} \in \Delta_k^N$, making the final output feasible for $\overline{\boldsymbol{P}}$.

“Pre-train + Fine-tune” Optimization. We propose a “pre-train + fine-tune” framework for learning the trainable weights of GNNs. Initially, the model is trained on a collection of pre-collected datasets to produce a pre-trained model. Subsequently, we fine-tune this pre-trained model for each specific testing instance. This approach equips the model with prior knowledge of graph structures during the pre-training phase, significantly reducing the overall solving time. Furthermore, it allows for out-of-distribution generalization due to the fine-tuning step.

In the pre-training phase, the trainable parameters $\boldsymbol{\Phi} := (\boldsymbol{\Phi}_1^{(1)}, \boldsymbol{\Phi}_2^{(1)}, \ldots, \boldsymbol{\Phi}_1^{(L)}, \boldsymbol{\Phi}_2^{(L)})$ are optimized using the Adam optimizer with *random initialization*, targeting the objective

$$\min_{\boldsymbol{\Phi}} \quad \mathcal{L}_{\text{pre-training}}(\boldsymbol{\Phi}) := \frac{1}{M}\sum_{m=1}^{M} f(\boldsymbol{H}_{\Phi}^{(L)}; \boldsymbol{W}_{\text{train}}^{(m)}),$$

where $\mathcal{D} := \{\boldsymbol{W}_{\text{train}}^{(1)}, \ldots, \boldsymbol{W}_{\text{train}}^{(M)}\}$ represents the pre-training dataset. In the fine-tuning phase, for a problem instance $\boldsymbol{W}_{\text{test}}$, the Adam optimizer seeks to solve

$$\min_{\boldsymbol{\Phi}} \quad \mathcal{L}_{\text{fine-tuning}}(\boldsymbol{\Phi}) := f(\boldsymbol{H}_{\Phi}^{(L)}; \boldsymbol{W}_{\text{test}}),$$

initialized with the pre-trained parameters.

Moreover, to enable the GNN model to fully adapt to specific problem instances, the pre-training phase can be omitted, enabling the model to be directly trained and tested on the same instance. While this direct approach may necessitate more computational time, it often results in improved performance regarding the objective function. Consequently, users can choose to include a pre-training phase based on the specific requirements of their application scenarios.

4. Experiments

4.1. Experimental Settings

We compare the performance of `ROS` against traditional methods as well as L2O algorithms for solving the Max-k-Cut problem. Additionally, we assess the impact of the “Pre-train” stage in the GNN parametrization-based optimization. The source code is available at `https://github.com/NetSysOpt/ROS`.

Baseline Algorithms. We denote our proposed algorithms by `ROS` and compare them against both traditional algorithms and L2O methods. When the pre-training step is skipped, we refer to our algorithm as `ROS-vanilla`. The following traditional Max-k-Cut algorithms are considered as baselines: (i) `GW` (Goemans & Williamson, 1995): an method with a 0.878-approximation guarantee based on semi-definite relaxation; (ii) `BQP` (Gui et al., 2019): a local search method designed for binary quadratic programs; (iii) `Genetic` (Li & Wang, 2016): a genetic algorithm specifically for Max-k-Cut problems; (iv) `MD`: a mirror descent algorithm that addresses the relaxed problem $\overline{\mathbf{P}}$ with a convergence tolerance at 10^{-8} and adopts the same random sampling procedure; (v) `LPI` (Goudet et al., 2024): an evolutionary algorithm featuring a large population organized across different islands; (vi) `MOH` (Ma & Hao, 2017): a heuristic algorithm based on multiple operator heuristics, employing various distinct search operators within the search phase. For the L2O method, we primarily examine the state-of-the-art baseline algorithms: (vii) `PI-GNN` (Schuetz et al., 2022): an unsupervised method for QUBO problems, which can model the weighted Max-Cut problem, delivering commendable performance. (viii) ECO-DQN (Barrett et al., 2020): a reinforcement L2O method introducing test-time exploratory refinement for Max-Cut problems. (ix) ANYCSP (Tönshoff et al., 2023): an unsupervised GNN-based search heuristic for CSPs, which can model the unweighted Max-k-Cut problem, leveraging a compact graph representation and global search action with the default time limit of 180 seconds.

Datasets. We conduct experiments on the following datasets.

- **r-Random regular graphs** (Schuetz et al., 2022): Each node has the same degree r. Edge weights are either 0 or 1.
- **Gset** (Ye, 2003): A well-known Max-k-Cut benchmark comprising toroidal, planar, and random graphs with $800 \sim 20,000$ nodes and edge densities between 2% and 6%. Edge weights are either 0 or ± 1.
- **COLOR** (Micheal, 2002): A collection of dense graphs derived from literary texts, where nodes represent characters and edges indicate co-occurrence. These graphs have large chromatic numbers ($\chi \approx 10$), making them suitable for Max-k-Cut. Edge weights are either 0 or 1.
- **Bitcoin-OTC** (Kumar et al., 2016): A real-world signed network with $5,881$ nodes and $35,592$ edges, weighted from -10 to 10, capturing trust relationships among Bitcoin users.

The construction of the training and testing datasets is summarized in Table 1. The training set consists of 500 3-regular, 500 5-regular graphs, and 500 7-regular graphs with 100 nodes each, corresponding to the cases $k = 2$, $k = 3$, and $k = 10$ respectively. The test set of random regular graphs includes 20 3-regular and 20 5-regular graphs for each $k \in \{2, 3\}$, with node counts of 100, 1,000, and 10,000. For the Gset benchmark, we evaluate both unweighted and weighted variants. The unweighted test set includes all Gset instances, with results reported in Tables 6 and 7 in Appendix D. For the weighted variant, we generate perturbations of the four largest Gset graphs (G70, G72, G77, G81) by multiplying each edge weight by $\sigma \sim \mathcal{U}[l, u]$, creating 10 perturbed instances per graph. We examine three distinct perturbation regimes: (i) mild perturbations ($[0.9, 1.1]$), (ii) moderate variations ($[0, 10]$), and (iii) extreme modifications ($[0, 100]$). The moderate perturbation results ($[0, 10]$) are presented in Table 3, with the remaining cases available in Appendix E. Additionally, we evaluate performance on three COLOR benchmark instances: anna, david, and huck.

Model Settings. ROS is designed as a two-layer GNN, with both the input and hidden dimensions set to 100. To address the issue of gradient vanishing, we apply graph normalization as proposed by Cai et al. (2021). The ROS model is pre-training using Adam with a learning rate of 10^{-2} for one epoch. During fine-tuning, the model is further optimized using the same Adam optimizer and learning rate, applying early stopping with a tolerance of 10^{-2} and patience of 100 iterations. Training terminates if no improvement is observed. Finally, in the random sampling stage, we execute Algorithm 1 for $T = 100$ trials and return the best solution.

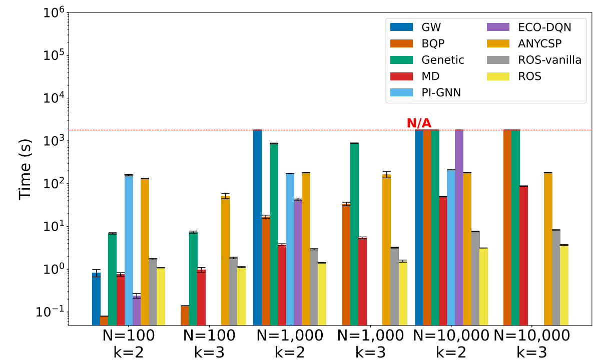

(a) Random regular graph

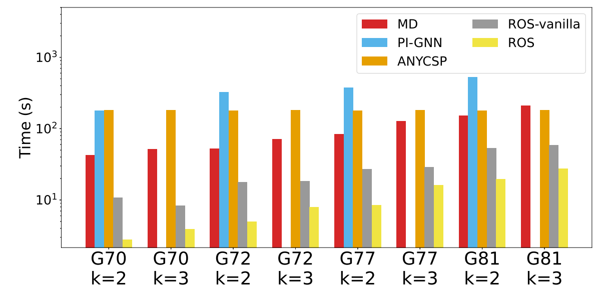

(b) Weighted Gset with perturbation ratio $[0, 10]$

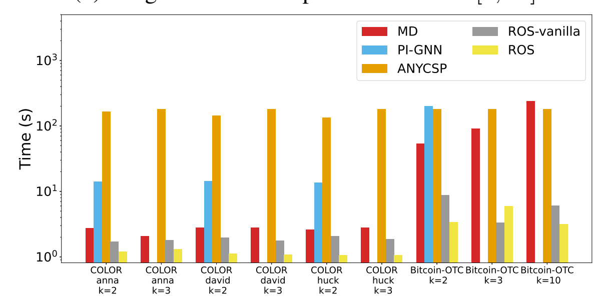

(c) COLOR datasets and Bitcoin-OTC datasets

Figure 2: The computational time comparison of Max-k-Cut problems.

Evaluation Configuration. All our experiments were conducted on an NVIDIA RTX 3090 GPU, using PyTorch 2.2.0.

Table 1: Statistics of the training and testing datasets.

	Dataset	Graph Type	N	# Graphs	Weight Type
Train	Random Regular Graph	regular	100	500	unweighted
Test	Random Regular Graph	regular	100, 1,000, 10,000	60	unweighted
	Gset	random, planar, toroidal	800 $\sim$ 20,000	71	unweighted, weighted
	COLOR	real-world	74, 87, 138	3	unweighted
	Bitcoin-OTC	real-world	5,881	1	weighted

Table 2: Cut value comparison of Max-k-Cut problems on random regular graphs.

Methods	N=100		N=1,000		N=10,000	
	$k=2$	$k=3$	$k=2$	$k=3$	$k=2$	$k=3$
GW	$130.20_{\pm 2.79}$	–	N/A	–	N/A	–
BQP	$131.55_{\pm 2.42}$	$239.70_{\pm 1.82}$	$1324.45_{\pm 6.34}$	$2419.15_{\pm 6.78}$	N/A	N/A
Genetic	$127.55_{\pm 2.82}$	$235.50_{\pm 3.15}$	$1136.65_{\pm 10.37}$	$2130.30_{\pm 8.49}$	N/A	N/A
MD	$127.20_{\pm 2.16}$	$235.50_{\pm 3.29}$	$1250.35_{\pm 11.21}$	$2344.85_{\pm 9.86}$	$12428.85_{\pm 26.13}$	$23341.20_{\pm 32.87}$
PI-GNN	$122.95_{\pm 3.83}$	–	$1210.45_{\pm 44.56}$	–	$12655.05_{\pm 94.25}$	–
ECO-DQN	$135.60_{\pm 1.53}$	–	$1366.20_{\pm 5.20}$	–	N/A	–
ANYCSP	$131.65_{\pm 3.35}$	$247.90_{\pm 0.89}$	$1366.05_{\pm 5.25}$	$2494.50_{\pm 2.99}$	$13692.35_{\pm 11.27}$	$24929.80_{\pm 7.53}$
ROS-vanilla	$132.80_{\pm 1.99}$	$243.20_{\pm 1.80}$	$1322.95_{\pm 6.57}$	$2443.9_{\pm 4.10}$	$13239.80_{\pm 14.71}$	$24413.30_{\pm 16.02}$
ROS	$128.20_{\pm 2.82}$	$240.30_{\pm 2.59}$	$1283.75_{\pm 6.89}$	$2405.75_{\pm 5.72}$	$12856.85_{\pm 26.50}$	$24085.95_{\pm 21.88}$

4.2. Performance Comparison against Baselines

4.2.1. Computational Time

We evaluated ROS against seven baseline algorithms: GW, BQP, Genetic, MD, PI-GNN, ECO-DQN, and ANYCSP on random regular graphs, comparing computational time for both Max-Cut and Max-3-Cut tasks. Experiments covered three problem scales: $N = 100$, $N = 1{,}000$, and $N = 10{,}000$, with results shown in Figure 2a. For larger instances, Figure 2b compares the scalable methods (MD, ANYCSP, and PI-GNN) on weighted Gset graphs ($N \geq 10{,}000$) with edge weight perturbations in $[0, 10]$. Figure 2c extends this comparison to real-world networks (COLOR and Bitcoin-OTC graphs). Instances marked "N/A" indicate timeout failures (30-minute limit). Complete results for unweighted Gset benchmarks, including comparisons with state-of-the-art methods LPI and MOH, are provided in Tables 6 and 7 (Appendix D).

The results depicted in Figure 2a indicate that ROS efficiently solves all problem instances within seconds, even for large problem sizes of $N = 10,000$. In terms of baseline performance, the approximation algorithm GW performs efficiently on instances with $N = 100$, but it struggles with larger sizes due to the substantial computational burden associated with solving the underlying semi-definite programming problem. Heuristic methods such as BQP and Genetic can manage cases up to $N = 1,000$ in a few hundred seconds, yet they fail to solve larger instances with $N = 10,000$ because of the high computational cost of each iteration. Notably, MD is the only traditional method capable of solving large instances within a reasonable time frame; however, when N reaches $10,000$, the computational time for MD approaches 15 times that of ROS. Regarding L2O methods, PI-GNN necessitates retraining and prediction for each instance, with test times exceeding dozens of seconds even for $N = 100$. ECO-DQN relies on expensive GNNs at each decision step and can not scale to large problem sizes of $N = 10,000$. ANYCSP needs hundreds of seconds even for $N = 100$ due to the global search operation and long sampling trajectory. In contrast, ROS solves these large instances in merely a few seconds throughout the experiments, requiring only 10% of the computational time utilized by other L2O baselines. Figure 2b and Figure 2c illustrate the results for the weighted Gset benchmark and real-world datasets, respectively, where ROS efficiently solves the largest instances in just a few seconds, while other methods take tens to hundreds of seconds for equivalent tasks. Remarkably, ROS utilizes only about 1% of the computational time required by PI-GNN.

4.2.2. Cut Value

We evaluate ROS's performance on random regular graphs, the Gset benchmark, and real-world datasets, measuring solution quality for Problem (1). Results appear in Tables 2 (random graphs), 3 (weighted Gset), and 4 (real-world data), where "–" denotes methods incompatible with Max-k-Cut problems.

Table 3: Cut value comparison of Max-k-Cut problems on weighted Gset instances, where the noise factor $\sigma \sim [0, 10]$.

Methods	G70 (N=10,000)		G72 (N=10,000)		G77 (N=14,000)		G81 (N=20,000)	
	$k=2$	$k=3$	$k=2$	$k=3$	$k=2$	$k=3$	$k=2$	$k=3$
GW	N/A	–	N/A	–	N/A	–	N/A	–
BQP	N/A	N/A	N/A	N/A	N/A	N/A	N/A	N/A
Genetic	N/A	N/A	N/A	N/A	N/A	N/A	N/A	N/A
MD	45490.21	49615.85	33449.49	38798.78	47671.94	55147.26	67403.00	78065.07
PI-GNN	44275.72	–	31469.65	–	44359.72	–	62439.97	–
ECO-DQN	N/A	–	N/A	–	N/A	–	N/A	–
ANYCSP	46420.48	48831.32	−280.74	−208.01	845.72	988.96	−13.52	271.01
ROS-vanilla	47140.07	49826.90	36697.11	42067.80	52226.53	59636.36	74051.42	84498.44
ROS	46707.60	49813.45	35733.11	40987.92	50790.44	58253.31	72057.24	82450.68

Table 4: Cut value comparison of Max-k-Cut problems on COLOR datasets and Bitcoin-OTC Datasets.

Methods	COLOR anna		COLOR david		COLOR huck		Bitcoin-OTC		
	$k=2$	$k=3$	$k=2$	$k=3$	$k=2$	$k=3$	$k=2$	$k=3$	$k=10$
MD	339	421	259	329	184	242	39076	47595	53563
PI-GNN	279	–	228	–	166	–	37216	–	–
ANYCSP	330	423	263	328	166	139	10431	14265	19372
ROS-vanilla	351	429	266	336	191	246	40576	48214	53758
ROS	351	423	266	324	191	242	39850	48980	53778

The results demonstrate that ROS consistently produces high-quality solutions for both $k = 2$ and $k = 3$ across all scales. While GW performs well for Max-Cut ($k = 2$) at $N = 100$, it fails to generalize to arbitrary k. Traditional methods like BQP and Genetic support $k = 3$ but often converge to suboptimal solutions. Although MD handles general k, it consistently underperforms ROS. Among learning-based methods, PI-GNN proves unsuitable for $k = 3$ due to QUBO incompatibility and unreliable heuristic rounding, while ECO-DQN lacks $k = 3$ support entirely. While ANYCSP achieves strong results on unweighted graphs, it cannot process weighted instances. These experiments collectively show that ROS offers superior generalizability and robustness for weighted Max-k-Cut tasks, outperforming both traditional and learning-based approaches in solution quality and flexibility.

To further assess ROS's scalability, we conduct comprehensive benchmarking against scalable baselines using challenging real-world datasets, including the COLOR and Bitcoin-OTC networks. The results in Table 4 demonstrate that both ROS and its simplified variant ROS-vanilla consistently outperform competing methods across most experimental settings. This performance advantage is particularly pronounced for the weighted Bitcoin-OTC instances, where our approach achieves superior solution quality while maintaining computational efficiency.

4.3. Effect of the "Pre-train" Stage in ROS

To evaluate the impact of the pre-training stage in ROS, we compared it with ROS-vanilla, which omits pre-training (see Section 3.3). We assessed both methods based on cut values and computational time. Figure 3 illustrates the ratios of these metrics between ROS-vanilla and ROS. In this figure, the horizontal axis represents the problem instances, while the left vertical axis (green bars) displays the ratio of objective function values, and the right vertical axis (red curve) indicates the ratio of computational times.

As shown in Figure 3a, ROS-vanilla achieves higher objective function values in most settings on the random regular graphs; however, its computational time is approximately 1.5 times greater than that of ROS. Thus, ROS demonstrates a faster solving speed compared to ROS-vanilla. Similarly, in experiments conducted on the Gset benchmark (Figure 3b), ROS reduces computational time by around 40% while maintaining performance comparable to that of ROS-vanilla. Notably, in the Max-3-Cut problem for the largest instance, G81, ROS effectively halves the solving time, showcasing the significant acceleration effect of pre-training. It is worth mentioning that the ROS model was pre-trained on random regular graphs with $N = 100$ and generalized well to regular graphs with $N = 1{,}000$ and $N = 10{,}000$, as well as to Gset problem instances of varying sizes and types. This illustrates ROS's capability to

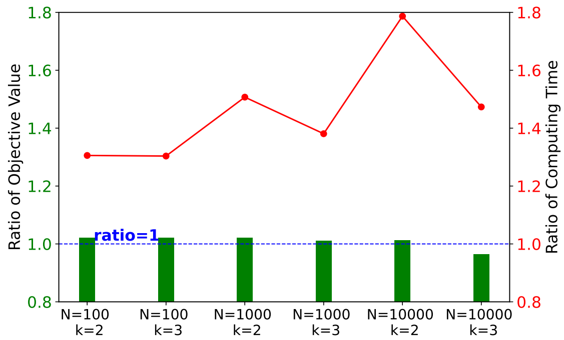

(a) Random regular graph

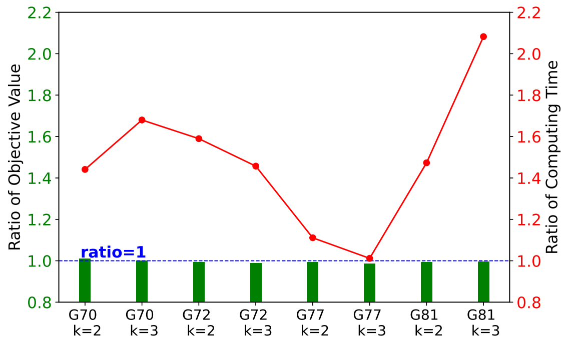

(b) Gset

Figure 3: The ratio of computational time and cut value comparison between `ROS-vanilla` and `ROS`.

generalize and accelerate the solving of large-scale problems across diverse graph types and sizes, emphasizing the strong out-of-distribution generalization afforded by pre-training.

In summary, while `ROS-vanilla` achieves slightly higher objective function values on individual instances, it requires longer solving times and struggles to generalize to other problem instances. This observation highlights the trade-off between a model's ability to generalize and its capacity to fit specific instances. Specifically, a model that fits individual instances exceptionally well may fail to generalize to new data, resulting in longer solving times. Conversely, a model that generalizes effectively may exhibit slightly weaker performance on specific instances, leading to a marginal decrease in objective function values. Therefore, the choice between these two training modes should be guided by the specific requirements of the application.

5. Conclusions

In this paper, we propose ROS, an efficient method for addressing the Max-k-Cut problem with arbitrary edge weights. Our approach begins by relaxing the constraints of the original discrete problem to probabilistic simplices. To effectively solve this relaxed problem, we propose an optimization algorithm based on GNN parametrization and incorporate transfer learning by leveraging pre-trained GNNs to warm-start the training process. After resolving the relaxed problem, we present a novel random sampling algorithm that maps the continuous solution back to a discrete form. By integrating geometric landscape analysis with statistical theory, we establish the consistency of function values between the continuous and discrete solutions. Experiments conducted on random regular graphs, the Gset benchmark, and real-world datasets demonstrate that our method is highly efficient for solving large-scale Max-k-Cut problems, requiring only a few seconds, even for instances with tens of thousands of variables. Furthermore, it exhibits robust generalization capabilities across both in-distribution and out-of-distribution instances, highlighting its effectiveness for large-scale optimization tasks. Exploring other sampling algorithms to further boost ROS performance is a future research direction. Moreover, the ROS framework with theoretical insights could be potentially extended to other graph-related combinatorial problems, and this direction is also worth investigating as future work.

Impact Statement

This paper presents work whose goal is to advance the field of Machine Learning. There are many potential societal consequences of our work, none of which we feel must be specifically highlighted here.

Acknowledgement

This work was supported by the National Key R&D Program of China under grant 2022YFA1003900. Ye Xue acknowledges support from the National Natural Science Foundation of China (Grant No. 62301334), the Guangdong Major Project of Basic and Applied Basic Research (No. 2023B0303000001), Akang Wang also acknowledges support from the National Natural Science Foundation of China (Grant No. 12301416), the Guangdong Basic and Applied Basic Research Foundation (Grant No. 2024A1515010306).

References

Andrade, C. E., Pessoa, L. S., and Stawiarski, S. The physical cell identity assignment problem: A practical optimization approach. *IEEE Transactions on Evolutionary Computation*, 28(2):282–292, 2024.

Bach, F. *Learning with Submodular Functions: A Convex Optimization Perspective*. Now Publishers Inc., Hanover, MA, USA, 2013. ISBN 1601987560.

Barrett, T., Clements, W., Foerster, J., and Lvovsky, A. Exploratory combinatorial optimization with reinforcement learning. *Proceedings of the AAAI Conference on Artificial Intelligence*, 34(04):3243–3250, 2020.

Barrett, T. D., Parsonson, C. W., and Laterre, A. Learning to solve combinatorial graph partitioning problems via efficient exploration. *arXiv preprint arXiv:2205.14105*, 2022.

Bengio, Y., Lodi, A., and Prouvost, A. Machine learning for combinatorial optimization: A methodological tour d'horizon. *European Journal of Operational Research*, 290(2):405–421, 2021. ISSN 0377-2217.

Bhowmick, A., Kosan, M., Huang, Z., Singh, A., and Medya, S. Dgcluster: A neural framework for attributed graph clustering via modularity maximization. *Proceedings of the AAAI Conference on Artificial Intelligence*, 38 (10):11069–11077, 2024.

Burer, S., Monteiro, R. D. C., and Zhang, Y. Rank-two relaxation heuristics for max-cut and other binary quadratic programs. *SIAM Journal on Optimization*, 12(2):503–521, 2002.

Cai, T., Luo, S., Xu, K., He, D., Liu, T.-Y., and Wang, L. Graphnorm: A principled approach to accelerating graph neural network training. In *Proceedings of the 38th International Conference on Machine Learning*, volume 139 of *Proceedings of Machine Learning Research*, pp. 1204–1215. PMLR, 18–24 Jul 2021.

Carlson, R. and Nemhauser, G. L. Scheduling to minimize interaction cost. *Operations Research*, 14(1):52–58, 1966.

Chen, M., Chen, Y., Du, Y., Wei, L., and Chen, Y. Heuristic algorithms based on deep reinforcement learning for quadratic unconstrained binary optimization. *Knowledge-Based Systems*, 207:106366, 2020. ISSN 0950-7051.

Chen, X., Liu, J., and Yin, W. Learning to optimize: A tutorial for continuous and mixed-integer optimization. *Science China Mathematics*, pp. 1–72, 2024.

Coja-Oghlan, A., Loick, P., Mezei, B. F., and Sorkin, G. B. The ising antiferromagnet and max cut on random regular graphs. *SIAM Journal on Discrete Mathematics*, 36(2): 1306–1342, 2022.

Cook, C., Zhao, H., Sato, T., Hiromoto, M., and Tan, S. X.-D. Gpu-based ising computing for solving max-cut combinatorial optimization problems. *Integration*, 69: 335–344, 2019. ISSN 0167-9260.

de Klerk, E., Pasechnik, D. V., and Warners, J. P. On approximate graph colouring and max-k-cut algorithms based on the θ-function. *Journal of Combinatorial Optimization*, 8:267–294, 2004.

De Simone, C., Diehl, M., Jünger, M., Mutzel, P., Reinelt, G., and Rinaldi, G. Exact ground states of ising spin glasses: New experimental results with a branch-and-cut algorithm. *Journal of Statistical Physics*, 80:487–496, 1995.

Eisenblätter, A. The semidefinite relaxation of the k-partition polytope is strong. In *Integer Programming and Combinatorial Optimization*, pp. 273–290, Berlin, Heidelberg, 2002. Springer Berlin Heidelberg.

Frieze, A. and Jerrum, M. Improved approximation algorithms for max k-cut and max bisection. *Algorithmica*, 18(1):67–81, 1997.

Garvardt, J., Grüttemeier, N., Komusiewicz, C., and Morawietz, N. Parameterized local search for max c-cut. In Elkind, E. (ed.), *Proceedings of the Thirty-Second International Joint Conference on Artificial Intelligence, IJCAI-23*, pp. 5586–5594. International Joint Conferences on Artificial Intelligence Organization, 8 2023. Main Track.

Gasse, M., Bowly, S., Cappart, Q., Charfreitag, J., Charlin, L., Chételat, D., Chmiela, A., Dumouchelle, J., Gleixner, A., Kazachkov, A. M., et al. The machine learning for combinatorial optimization competition (ml4co): Results and insights. In *NeurIPS 2021 competitions and demonstrations track*, pp. 220–231. PMLR, 2022.

Ghaddar, B., Anjos, M. F., and Liers, F. A branch-and-cut algorithm based on semidefinite programming for the minimum k-partition problem. *Annals of Operations Research*, 188(1):155–174, 2011.

Goemans, M. X. and Williamson, D. P. Improved approximation algorithms for maximum cut and satisfiability problems using semidefinite programming. *Journal of the ACM (JACM)*, 42(6):1115–1145, 1995.

Goudet, O., Goëffon, A., and Hao, J.-K. A large population island framework for the unconstrained binary quadratic problem. *Computers & Operations Research*, 168:106684, 2024. ISSN 0305-0548.

Gui, J., Jiang, Z., and Gao, S. Pci planning based on binary quadratic programming in lte/lte-a networks. *IEEE Access*, 7:203–214, 2019.

Hojny, C., Joormann, I., Lüthen, H., and Schmidt, M. Mixed-integer programming techniques for the connected max-k-cut problem. *Mathematical Programming Computation*, 13(1):75–132, 2021.

Karalias, N. and Loukas, A. Erdos goes neural: an unsupervised learning framework for combinatorial optimization on graphs. In *Advances in Neural Information Processing Systems*, volume 33, pp. 6659–6672. Curran Associates, Inc., 2020.

Karp, R. M. *Reducibility among Combinatorial Problems*, pp. 85–103. Springer US, Boston, MA, 1972. ISBN 978-1-4684-2001-2.

Khalil, E., Dai, H., Zhang, Y., Dilkina, B., and Song, L. Learning combinatorial optimization algorithms over graphs. In *Advances in Neural Information Processing Systems*, volume 30. Curran Associates, Inc., 2017.

Kumar, S., Spezzano, F., Subrahmanian, V. S., and Faloutsos, C. Edge weight prediction in weighted signed networks. In *2016 IEEE 16th International Conference on Data Mining (ICDM)*, pp. 221–230, 2016.

Li, P. and Wang, J. Pci planning method based on genetic algorithm in lte network. *Telecommunications Science*, 32(3):2016082, 2016.

Ly, A., Sawhney, R., and Chugunova, M. Data clustering and visualization with recursive goemans-williamson maxcut algorithm. In *2023 International Conference on Computational Science and Computational Intelligence (CSCI)*, pp. 496–500. IEEE, 2023.

Ma, F. and Hao, J.-K. A multiple search operator heuristic for the max-k-cut problem. *Annals of Operations Research*, 248:365–403, 2017.

Michael, R., Bartels, S., González-Duque, M., Zainchkovskyy, Y., Frellsen, J., Hauberg, S., and Boomsma, W. A continuous relaxation for discrete bayesian optimization. *arXiv preprint arXiv:2404.17452*, 2024.

Micheal, T. The color datasets. https://mat.tepper.cmu.edu/COLOR02/, 2002.

Morris, C., Ritzert, M., Fey, M., Hamilton, W. L., Lenssen, J. E., Rattan, G., and Grohe, M. Weisfeiler and leman go neural: Higher-order graph neural networks. *Proceedings of the AAAI Conference on Artificial Intelligence*, 33(01): 4602–4609, Jul. 2019.

Nath, A. and Kuhnle, A. A benchmark for maximum cut: Towards standardization of the evaluation of learned heuristics for combinatorial optimization. *arXiv preprint arXiv:2406.11897*, 2024.

Poland, J. and Zeugmann, T. Clustering pairwise distances with missing data: Maximum cuts versus normalized cuts. In *International Conference on Discovery Science*, pp. 197–208. Springer, 2006.

Schuetz, M. J., Brubaker, J. K., and Katzgraber, H. G. Combinatorial optimization with physics-inspired graph neural networks. *Nature Machine Intelligence*, 4(4):367–377, 2022.

Shah, R., Jain, K., Manchanda, S., Medya, S., and Ranu, S. Neurocut: A neural approach for robust graph partitioning. In *Proceedings of the 30th ACM SIGKDD Conference on Knowledge Discovery and Data Mining*, KDD '24, pp. 2584–2595, New York, NY, USA, 2024. Association for Computing Machinery. ISBN 9798400704901.

Shinde, N., Narayanan, V., and Saunderson, J. Memory-efficient approximation algorithms for max-k-cut and correlation clustering. In *Advances in Neural Information Processing Systems*, volume 34, pp. 8269–8281. Curran Associates, Inc., 2021.

Tönshoff, J., Ritzert, M., Wolf, H., and Grohe, M. Graph neural networks for maximum constraint satisfaction. *Frontiers in artificial intelligence*, 3:580607, 2021.

Tönshoff, J., Kisin, B., Lindner, J., and Grohe, M. One model, any csp: Graph neural networks as fast global search heuristics for constraint satisfaction. In *Proceedings of the Thirty-Second International Joint Conference on Artificial Intelligence, IJCAI-23*, pp. 4280–4288. International Joint Conferences on Artificial Intelligence Organization, 8 2023. Main Track.

Tsitsulin, A., Palowitch, J., Perozzi, B., and Müller, E. Graph clustering with graph neural networks. *Journal of Machine Learning Research*, 24(127):1–21, 2023.

Ye, Y. The gset dataset. https://web.stanford.edu/~yyye/yyye/Gset/, 2003.

A. Related Works

Relaxation-based methods have been central to the algorithmic design for Max-Cut and its generalizations. In Table 5, we compare our proposed probability simplex relaxation with several representative approaches along key dimensions: variable complexity (# Var.), applicability to general Max-k-Cut, polynomial-time solvability, objective value consistency with the original problem, and scalability to large instances.

Table 5: Comparison between Different Relaxations

Relaxation	**# Var.**	**Max-k-Cut**	**Polynomial Solvable?**	**Obj. Value Consistency?**	**Scalable?**
Lovasz Extension (Bach, 2013)	$\mathcal{O}(N)$	✗	✗	✓	✓
SDP Relaxation (Goemans & Williamson, 1995)	$\mathcal{O}(N^2)$	✗	✓	✗	✗
SDP Relaxation (Frieze & Jerrum, 1997)	$\mathcal{O}(N \times k)$	✓	✓	✗	✗
Rank-2 Relaxation (Burer et al., 2002)	$\mathcal{O}(N)$	✗	✗	✗	✓
QUBO Relaxation (Andrade et al., 2024)	$\mathcal{O}(N)$	✗	✗	✗	✓
Probability Simplex Relaxation (ours)	$\mathcal{O}(N \times k)$	✓	✗	✓	✓

The Lovász extension (Bach, 2013), originally designed for submodular optimization, admits scalable convex formulations but does not extend naturally to general Max-k-Cut problems. Seminal SDP-based methods, such as Goemans-Williamson (Goemans & Williamson, 1995) for Max-Cut and its k-way extension (Frieze & Jerrum, 1997), offer polynomial-time approximation guarantees. However, their reliance on large-scale semidefinite programming limits practical scalability and makes them less effective on modern large-scale instances. Non-convex formulations, including the rank-2 relaxation (Burer et al., 2002) and QUBO-based relaxation (Andrade et al., 2024), provide scalable alternatives for Max-Cut but lack theoretical guarantees for Max-k-Cut and are typically solved locally. These methods often exhibit poor objective consistency and limited generalization.

In contrast, our probability simplex relaxation introduces a non-convex yet tractable formulation for Max-k-Cut with $\mathcal{O}(N \times k)$ variables. While it is not globally solvable in polynomial time, its optimal value aligns exactly with that of the original Max-k-Cut problem. Empirically, our GNN-based solver produces high-quality fractional solutions, which serve as effective initializations for randomized sampling. Overall, the proposed relaxation strikes a favorable balance between expressiveness, consistency, and scalability, offering a practical and theoretically grounded solution framework for large-scale Max-k-Cut problems.

B. Proof of Theorem 3.2

Proof. Before proceeding with the proof of Theorem 3.2, we first define the neighborhood of a vector $\bar{\boldsymbol{x}} \in \Delta_k$, and establish results of Lemma B.2 and Lemma B.3.

Definition B.1. Let $\bar{\boldsymbol{x}} = (\bar{\boldsymbol{x}}_1, \cdots, \bar{\boldsymbol{x}}_k)$ denote a point in Δ_k. We define the neighborhood induced by $\bar{\boldsymbol{x}}$ as follows:

$$\widetilde{\mathcal{N}}(\bar{\boldsymbol{x}}) := \left\{ (\boldsymbol{x}_1, \cdots, \boldsymbol{x}_k) \in \Delta_k \,\middle|\, \sum_{j \in \mathcal{K}(\bar{\boldsymbol{x}})} \boldsymbol{x}_j = 1 \right\},$$

where $\mathcal{K}(\bar{\boldsymbol{x}}) = \{j \in \{1, \cdots, k\} \mid \bar{\boldsymbol{x}}_j > 0\}$.

Lemma B.2. *Given $\boldsymbol{X}_{\cdot i} \in \widetilde{\mathcal{N}}(\boldsymbol{X}^\star_{\cdot i})$, it follows that*

$$\mathcal{K}(\boldsymbol{X}_{\cdot i}) \subseteq \mathcal{K}(\boldsymbol{X}^\star_{\cdot i}).$$

Proof. Suppose there exists $j \in \mathcal{K}(\boldsymbol{X}_{\cdot i})$ such that $j \notin \mathcal{K}(\boldsymbol{X}^\star_{\cdot i})$, implying $\boldsymbol{X}_{ji} > 0$ and $\boldsymbol{X}^\star_{ji} = 0$.

We then have

$$\sum_{l \in \mathcal{K}(\boldsymbol{X}^\star_{\cdot i})} \boldsymbol{X}_{li} + \boldsymbol{X}_{ji} \leq \sum_{l=1}^{k} \boldsymbol{X}_{li} = 1,$$

which leads to

$$\sum_{l \in \mathcal{K}(\boldsymbol{X}^\star_{\cdot i})} \boldsymbol{X}_{li} \leq 1 - \boldsymbol{X}_{ji} < 1,$$

contradicting with the fact that $\boldsymbol{X}_{\cdot i} \in \widetilde{\mathcal{N}}(\boldsymbol{X}^\star_{\cdot i})$. $\square$

Lemma B.3. *Let $\boldsymbol{X}^\star$ be a globally optimal solution to $\overline{\boldsymbol{P}}$, then*

$$f(\boldsymbol{X}; \boldsymbol{W}) = f(\boldsymbol{X}^\star; \boldsymbol{W}),$$

where $\boldsymbol{X}$ has only the i^{th} column $\boldsymbol{X}_{\cdot i} \in \widetilde{\mathcal{N}}(\boldsymbol{X}^\star_{\cdot i})$, and other columns are identical to those of $\boldsymbol{X}^\star$. Moreover, $\boldsymbol{X}$ is also a globally optimal solution to $\bar{\boldsymbol{P}}$.

Proof. The fact that $\boldsymbol{X}$ is a globally optimal solution to $\bar{\boldsymbol{P}}$ follows directly from the equality $f(\boldsymbol{X}; \boldsymbol{W}) = f(\boldsymbol{X}^\star; \boldsymbol{W})$. Thus, it suffices to prove this equality. Consider that $\boldsymbol{X}^\star$ and $\boldsymbol{X}$ differ only in the i^{th} column, and $\boldsymbol{X}_{\cdot i} \in \widetilde{\mathcal{N}}(\boldsymbol{X}^\star_{\cdot i})$. We can rewrite the objective value function as

$$f(\boldsymbol{X}; \boldsymbol{W}) = g(\boldsymbol{X}_{\cdot i}; \boldsymbol{X}_{\cdot -i}) + h(\boldsymbol{X}_{\cdot -i}),$$

where $\boldsymbol{X}_{\cdot -i}$ represents all column vectors of $\boldsymbol{X}$ except the i^{th} column. The functions g and h are defined as follows:

$$g(\boldsymbol{X}_{\cdot i}; \boldsymbol{X}_{\cdot -i}) = \sum_{j=1}^{N} \boldsymbol{W}_{ij} \boldsymbol{X}_{\cdot i}^\top \boldsymbol{X}_{\cdot j} + \sum_{j=1}^{N} \boldsymbol{W}_{ji} \boldsymbol{X}_{\cdot j}^\top \boldsymbol{X}_{\cdot i} - \boldsymbol{W}_{ii} \boldsymbol{X}_{\cdot i}^\top \boldsymbol{X}_{\cdot i},$$

$$h(\boldsymbol{X}_{\cdot -i}) = \sum_{l=1, l\neq i}^{N} \sum_{j=1, j\neq i}^{N} \boldsymbol{W}_{lj} \boldsymbol{X}_{\cdot l}^\top \boldsymbol{X}_{\cdot j}$$

To establish that $f(\boldsymbol{X}; \boldsymbol{W}) = f(\boldsymbol{X}^\star; \boldsymbol{W})$, it suffices to show that

$$g(\boldsymbol{X}_{\cdot i}; \boldsymbol{X}_{\cdot -i}) = g(\boldsymbol{X}^\star_{\cdot i}; \boldsymbol{X}_{\cdot -i})$$

as $\boldsymbol{X}_{\cdot -i} = \boldsymbol{X}^\star_{\cdot -i}$.

Rewriting $g(\boldsymbol{X}_{\cdot i}; \boldsymbol{X}_{\cdot -i})$, we obtain

$$\begin{aligned} g(\boldsymbol{X}_{\cdot i}; \boldsymbol{X}_{\cdot -i}) &= \sum_{j=1}^{N} \boldsymbol{W}_{ij} \boldsymbol{X}_{\cdot i}^\top \boldsymbol{X}_{\cdot j} + \sum_{j=1}^{N} \boldsymbol{W}_{ji} \boldsymbol{X}_{\cdot j}^\top \boldsymbol{X}_{\cdot i} \\ &= 2 \sum_{j=1}^{N} \boldsymbol{W}_{ij} \boldsymbol{X}_{\cdot i}^\top \boldsymbol{X}_{\cdot j} \\ &= 2 \boldsymbol{X}_{\cdot i}^\top \sum_{j=1, j\neq i}^{N} \boldsymbol{W}_{ij} \boldsymbol{X}_{\cdot j} \\ &= 2 \boldsymbol{X}_{\cdot i}^\top \boldsymbol{Y}_{\cdot i}, \end{aligned}$$

where $\boldsymbol{Y}_{\cdot i} := \sum_{j=1, j\neq i}^{N} \boldsymbol{W}_{ij} \boldsymbol{X}_{\cdot j}$.

If $|\mathcal{K}(\boldsymbol{X}^\star_{\cdot i})| = 1$, then there is only one non-zero element in $\boldsymbol{X}^\star_{\cdot i}$ equal to one. Therefore, $g(\boldsymbol{X}^\star_{\cdot i}; \boldsymbol{X}_{\cdot -i}) = g(\boldsymbol{X}_{\cdot i}; \boldsymbol{X}_{\cdot -i})$ since $\boldsymbol{X}_{\cdot i} = \boldsymbol{X}^\star_{\cdot i}$.

For the case where $|\mathcal{K}(\boldsymbol{X}^\star_{\cdot i})| > 1$, we consider any indices $j, l \in \mathcal{K}(\boldsymbol{X}^\star_{\cdot i})$ such that $\boldsymbol{X}^\star_{ji}, \boldsymbol{X}^\star_{li} \in (0, 1)$. Then, there exists $\epsilon > 0$ such that we can construct a point $\widetilde{\boldsymbol{x}} \in \Delta_k$ where the j^{th} element is set to $\boldsymbol{X}^\star_{ji} - \epsilon$, the l^{th} element is set to $\boldsymbol{X}^\star_{li} + \epsilon$, and all other elements remain the same as in $\boldsymbol{X}^\star_{\cdot i}$. Since $\boldsymbol{X}^\star$ is a globally optimum of the function $f(\boldsymbol{X}; \boldsymbol{W})$, it follows that $\boldsymbol{X}^\star_{\cdot i}$ is also a global optimum for the function $g(\boldsymbol{X}^\star_{\cdot i}; \boldsymbol{X}_{\cdot -i})$. Thus, we have

$$\begin{aligned} g(\boldsymbol{X}^\star_{\cdot i}; \boldsymbol{X}_{\cdot -i}) &\leq g(\widetilde{\boldsymbol{x}}; \boldsymbol{X}_{\cdot -i}) \\ \boldsymbol{X}^{\star\top}_{\cdot i} \boldsymbol{Y}_{\cdot i} &\leq \widetilde{\boldsymbol{x}}^\top \boldsymbol{Y}_{\cdot i} \\ &= \boldsymbol{X}^{\star\top}_{\cdot i} \boldsymbol{Y}_{\cdot i} - \epsilon \boldsymbol{Y}_{ji} + \epsilon \boldsymbol{Y}_{li}, \end{aligned}$$

which leads to the inequality

$$\boldsymbol{Y}_{ji} \leq \boldsymbol{Y}_{li}. \tag{3}$$

Next, we can similarly construct another point $\hat{\boldsymbol{x}} \in \Delta_k$ with its j^{th} element equal to $\boldsymbol{X}^\star_{ji} + \epsilon$, the k^{th} element equal to $\boldsymbol{X}^\star_{ki} - \epsilon$, and all other elements remain the same as in $\boldsymbol{X}^\star_{\cdot i}$. Subsequently, we can also derive that

$$\begin{aligned} g(\boldsymbol{X}^\star_{\cdot i}; \boldsymbol{X}_{\cdot -i}) &\leq g(\hat{\boldsymbol{x}}; \boldsymbol{X}_{\cdot -i}) \\ &= \boldsymbol{X}^{\star\top}_{\cdot i} \boldsymbol{Y}_{\cdot i} + \epsilon \boldsymbol{Y}_{ji} - \epsilon \boldsymbol{Y}_{li}, \end{aligned}$$

which leads to another inequality

$$\boldsymbol{Y}_{li} \leq \boldsymbol{Y}_{ji}. \tag{4}$$

Consequently, combined inequalities (3) and (4), we have

$$\boldsymbol{Y}_{ji} = \boldsymbol{Y}_{li},$$

for $j, l \in \mathcal{K}(\boldsymbol{X}^\star_{\cdot i})$.

From this, we can deduce that

$$\boldsymbol{Y}_{j_1 i} = \boldsymbol{Y}_{j_2 i} = \cdots = \boldsymbol{Y}_{j_{|\mathcal{K}(\boldsymbol{X}^\star_{\cdot i})|} i} = t,$$

where $j_1, \cdots, j_{|\mathcal{K}(\boldsymbol{X}^\star_{\cdot i})|} \in \mathcal{K}(\boldsymbol{X}^\star_{\cdot i})$.

Next, we find that

$$\begin{aligned} g(\boldsymbol{X}^\star_{\cdot i}; \boldsymbol{X}_{\cdot -i}) &= 2\boldsymbol{X}^{\star\top}_{\cdot i} \boldsymbol{Y}_{\cdot i} \\ &= 2\sum_{j=1}^{k} \boldsymbol{X}^\star_{ji} \boldsymbol{Y}_{ji} \\ &= 2 \sum_{j=1, j \in \mathcal{K}(\boldsymbol{X}^\star_{\cdot i})}^{N} \boldsymbol{X}^\star_{ji} \boldsymbol{Y}_{ji} \\ &= 2t \sum_{j=1, j \in \mathcal{K}(\boldsymbol{X}^\star_{\cdot i})}^{N} \boldsymbol{X}^\star_{ji} \\ &= 2t. \end{aligned}$$

Similarly, we have

$$\begin{aligned} g(\boldsymbol{X}_{\cdot i}; \boldsymbol{X}_{\cdot -i}) &= 2\boldsymbol{X}^{\top}_{\cdot i} \boldsymbol{Y}_{\cdot i} \\ &= 2\sum_{j=1}^{k} \boldsymbol{X}_{ji} \boldsymbol{Y}_{ji} \\ &= 2 \sum_{j=1, j \in \mathcal{K}(\boldsymbol{X}_{\cdot i})} \boldsymbol{X}_{ji} \boldsymbol{Y}_{ji} \\ &\overset{\text{Lemma B.2}}{=} 2t \sum_{j=1, j \in \mathcal{K}(\boldsymbol{X}_{\cdot i})} \boldsymbol{X}_{ji} \\ &= 2t \end{aligned}$$

Accordingly, we conclude that

$$g(\boldsymbol{X}_{\cdot i}; \boldsymbol{X}_{\cdot -i}) = g(\boldsymbol{X}^\star_{\cdot i}; \boldsymbol{X}_{\cdot -i}),$$

which leads us to the result

$$f(\boldsymbol{X}; \boldsymbol{W}) = f(\boldsymbol{X}^\star; \boldsymbol{W}),$$

where $\boldsymbol{X}_{\cdot i} \in \widetilde{\mathcal{N}}(\boldsymbol{X}^\star_{\cdot i})$, $\boldsymbol{X}_{\cdot -i} = \boldsymbol{X}^\star_{\cdot -i}$. $\square$

Accordingly, for any $\boldsymbol{X} \in \mathcal{N}(\boldsymbol{X}^\star)$, we iteratively apply Lemma B.3 to each column of $\boldsymbol{X}^\star$ while holding the other columns fixed, thereby proving Theorem 3.2.

□

C. Proof of Theorem 3.3

Proof. Based on $\overline{\boldsymbol{X}}$, we can construct the random variable $\widetilde{\boldsymbol{X}}$, where $\widetilde{\boldsymbol{X}}_{\cdot i} \sim \text{Cat}(\boldsymbol{x}; \boldsymbol{p} = \overline{\boldsymbol{X}}_{\cdot i})$. The probability mass function is given by

$$\mathbf{P}(\widetilde{\boldsymbol{X}}_{\cdot i} = \boldsymbol{e}_\ell) = \overline{\boldsymbol{X}}_{\ell i}, \tag{5}$$

where $\ell = 1, \cdots, k$.

Next, we have

$$\begin{aligned}
\mathbb{E}_{\widetilde{\boldsymbol{X}}}[f(\widetilde{\boldsymbol{X}}; \boldsymbol{W})] = \mathbb{E}_{\widetilde{\boldsymbol{X}}}[\widetilde{\boldsymbol{X}} \boldsymbol{W} \widetilde{\boldsymbol{X}}^\top] &= \mathbb{E}_{\widetilde{\boldsymbol{X}}}[\sum_{i=1}^N \sum_{j=1}^N \boldsymbol{W}_{ij} \widetilde{\boldsymbol{X}}_{\cdot i}^\top \widetilde{\boldsymbol{X}}_{\cdot j}] \\
&= \sum_{i=1}^N \sum_{j=1}^N \boldsymbol{W}_{ij} \mathbb{E}_{\widetilde{\boldsymbol{X}}_{\cdot i} \widetilde{\boldsymbol{X}}_{\cdot j}}[\widetilde{\boldsymbol{X}}_{\cdot i}^\top \widetilde{\boldsymbol{X}}_{\cdot j}] \\
&= \sum_{i=1}^N \sum_{j=1}^N \boldsymbol{W}_{ij} \mathbb{E}_{\widetilde{\boldsymbol{X}}_{\cdot i} \widetilde{\boldsymbol{X}}_{\cdot j}}[\mathbb{1}(\widetilde{\boldsymbol{X}}_{\cdot i} = \widetilde{\boldsymbol{X}}_{\cdot j})] \\
&= \sum_{i=1}^N \sum_{j=1}^N \boldsymbol{W}_{ij} \mathbb{P}(\widetilde{\boldsymbol{X}}_{\cdot i} = \widetilde{\boldsymbol{X}}_{\cdot j}) \\
&= \sum_{i=1}^N \sum_{j=1, j \neq i}^N \boldsymbol{W}_{ij} \mathbb{P}(\widetilde{\boldsymbol{X}}_{\cdot i} = \widetilde{\boldsymbol{X}}_{\cdot j}).
\end{aligned} \tag{6}$$

Since $\widetilde{\boldsymbol{X}}_{\cdot i}$ and $\widetilde{\boldsymbol{X}}_{\cdot j}$ are independent for $i \neq j$, we have

$$\begin{aligned}
\mathbb{P}(\widetilde{\boldsymbol{X}}_{\cdot i} = \widetilde{\boldsymbol{X}}_{\cdot j}) &= \sum_{\ell=1}^k \mathbb{P}(\widetilde{\boldsymbol{X}}_{\cdot i} = \widetilde{\boldsymbol{X}}_{\cdot j} = \boldsymbol{e}_\ell) \\
&= \sum_{\ell=1}^k \mathbb{P}(\widetilde{\boldsymbol{X}}_{\cdot i} = \boldsymbol{e}_\ell, \widetilde{\boldsymbol{X}}_{\cdot j} = \boldsymbol{e}_\ell) \\
&= \sum_{\ell=1}^k \mathbb{P}(\widetilde{\boldsymbol{X}}_{\cdot i} = \boldsymbol{e}_\ell) \mathbb{P}(\widetilde{\boldsymbol{X}}_{\cdot j} = \boldsymbol{e}_\ell) \\
&= \sum_{\ell=1}^k \overline{\boldsymbol{X}}_{\ell i} \overline{\boldsymbol{X}}_{\ell j} \\
&= \overline{\boldsymbol{X}}_{\cdot i}^\top \overline{\boldsymbol{X}}_{\cdot j}.
\end{aligned} \tag{7}$$

Substitute (7) into (6), we obtain

$$\mathbb{E}_{\widetilde{\boldsymbol{X}}}[f(\widetilde{\boldsymbol{X}}; \boldsymbol{W})] = \sum_{i=1}^N \sum_{j=1}^N \boldsymbol{W}_{ij} \overline{\boldsymbol{X}}_{\cdot i}^\top \overline{\boldsymbol{X}}_{\cdot j} = f(\overline{\boldsymbol{X}}; \boldsymbol{W}). \tag{8}$$

□

D. The Results on Unweighted Gset Instances

Table 6: Complete results on Gset instances for Max-Cut.

Instance	$\lvert\mathcal{V}\rvert$	$\lvert\mathcal{E}\rvert$	GW		MD		PI-GNN		Genetic		BQP		ECO-DQN		ANYCSP		MOH		LPI		ROS-vanilla		ROS	
			Obj. ↑	Time (s) ↓	Obj. ↑	Time (s) ↓	Obj. ↑	Time (s) ↓	Obj. ↑	Time (s) ↓	Obj. ↑	Time (s) ↓	Obj. ↑	Time (s) ↓	Obj. ↑	Time (s) ↓	Obj. ↑	Time (s) ↓	Obj. ↑	Time (s) ↓	Obj. ↑	Time (s) ↓	Obj. ↑	Time (s) ↓
G1	800	19176	11299	1228.0	11320	5.1	10680	214.3	10929	587.4	11406	11.3	11482	23.4	11574	180.1	11624	1.5	11624	7	11423	2.6	11395	1.7
G2	800	19176	11299	1225.4	11255	5.3	10533	212.7	10926	588.3	11426	11.7	11516	25.2	11591	180.1	11620	4.6	11620	8	11462	2.6	11467	1.8
G3	800	19176	11289	1243.2	11222	5.3	10532	215.1	10933	596.8	11397	11.0	11543	26.1	11591	180.1	11622	1.3	11622	10	11510	2.7	11370	1.9
G4	800	19176	11207	1217.8	11280	4.8	10805	216.0	10945	580.5	11430	11.2	11522	26.8	11596	180.1	11646	5.2	11646	7	11416	2.6	11459	2.1
G5	800	19176	11256	1261.8	11156	3.7	10417	214.1	10869	598.2	11406	11.0	11485	24.2	11575	180.1	11631	1.0	11631	7	11505	2.6	11408	1.7
G6	800	19176	1776	1261.6	1755	6.9	1748	214.4	1435	581.2	1991	11.4	2095	23.3	2130	180.1	2178	3.0	2178	14	1994	2.5	1907	1.7
G7	800	19176	1694	1336.4	1635	5.9	1524	215.4	1273	587.5	1780	11.1	1957	25.5	1972	180.1	2006	3.0	2006	7	1802	2.6	1804	1.8
G8	800	19176	1693	1235.2	1651	6.1	1566	215.4	1241	591.8	1758	11.1	1955	25.5	1974	180.1	2005	5.7	2005	10	1876	2.8	1775	1.8
G9	800	19176	1676	1215.0	1720	8.0	1545	211.7	1345	582.3	1845	14.6	2044	26.8	2006	180.1	2054	3.2	2054	13	1839	2.6	1876	1.9
G10	800	19176	1675	1227.3	1700	7.3	1445	212.7	1313	589.5	1816	10.9	1930	27.1	1953	180.1	2000	68.1	2000	10	1811	2.6	1755	1.8
G11	800	1600	N/A	N/A	466	3.0	464	216.2	406	509.4	540	11.0	545	25.6	548	180.1	564	0.2	564	11	496	1.8	494	1.5
G12	800	1600	N/A	N/A	466	2.4	470	215.0	388	514.8	534	11.0	541	27.2	542	180.1	556	3.5	556	16	498	1.9	494	1.4
G13	800	1600	N/A	N/A	486	3.0	480	214.2	426	520.0	560	10.8	565	26.9	568	180.1	582	0.9	582	23	518	1.9	524	1.5
G14	800	4694	2942	1716.6	2930	3.1	2484	211.5	2855	564.2	2985	11.1	2807	23.4	3036	180.1	3064	251.3	3064	119	2932	1.5	2953	1.8
G15	800	4661	N/A	N/A	2932	3.1	2416	213.0	2836	547.7	2966	11.1	2741	26.2	3014	180.1	3050	52.2	3050	80	2920	1.8	2871	1.4
G16	800	4672	N/A	N/A	2937	3.8	2604	212.9	2848	541.3	2987	14.3	2757	26.8	3018	180.1	3052	93.7	3052	69	2917	1.7	2916	1.3
G17	800	4667	2916	1738.2	2922	3.3	2456	186.7	2829	558.9	2967	12.1	2754	25.8	3027	180.1	3047	129.5	3047	104	2932	1.9	2914	1.5
G18	800	4694	838	871.7	825	3.7	763	212.9	643	567.0	922	11.2	925	25.6	966	180.1	992	112.7	992	40	903	2.1	905	1.7
G19	800	4661	763	1245.4	740	3.6	725	206.5	571	571.2	816	11.4	828	27.2	881	180.1	906	266.9	906	49	808	2	772	1.5
G20	800	4672	781	1015.6	767	3.5	740	213.4	633	565.8	860	11.9	897	28.6	925	180.1	941	43.7	941	31	843	2.1	788	1.8
G21	800	4667	821	1350.3	784	3.0	740	209.3	620	572.2	837	14.1	864	25.2	925	180.1	931	155.3	931	32	858	2.1	848	1.6
G22	2000	19990	N/A	N/A	12777	12.2	12283	212.9	N/A	N/A	13004	95.6	13169	198.4	13280	180.1	13359	352.4	13359	413	13028	2.6	13007	2.7
G23	2000	19990	N/A	N/A	12688	10.2	12314	211.7	N/A	N/A	12958	95.6	13096	196.7	13297	180.1	13344	433.8	13342	150	13048	2.9	12936	1.9
G24	2000	19990	N/A	N/A	12721	10.0	11606	214.5	N/A	N/A	13002	95.0	13096	349.2	13284	180.1	13337	777.9	13337	234	13035	1.9	12933	2.4
G25	2000	19990	N/A	N/A	12725	11.7	12233	214.3	N/A	N/A	12968	102.6	13146	202.6	13279	180.1	13340	442.5	13340	258	13040	2	12947	1.9
G26	2000	19990	N/A	N/A	12725	10.8	12141	217.2	N/A	N/A	12966	96.9	13126	201.4	13253	180.1	13328	535.1	13328	291	13054	2.5	12954	3.5
G27	2000	19990	N/A	N/A	2632	11.2	2509	216.3	N/A	N/A	3062	98.9	3212	200.2	3300	180.1	3341	42.3	3341	152	2993	2.8	2971	2.1
G28	2000	19990	N/A	N/A	2762	11.2	2563	214.9	N/A	N/A	2963	96.8	3160	201.1	3265	180.1	3298	707.2	3298	197	2985	2.6	2923	1.9
G29	2000	19990	N/A	N/A	2736	12.3	2578	216.5	N/A	N/A	3044	96.4	3312	204.3	3348	180.1	3405	555.2	3405	293	3056	2.9	3089	1.9
G30	2000	19990	N/A	N/A	2774	11.7	2559	214.3	N/A	N/A	3074	99.3	3287	200.0	3363	180.1	3413	330.5	3413	410	3004	2.8	3025	2.9
G31	2000	19990	N/A	N/A	2736	11.5	2539	216.3	N/A	N/A	2998	96.3	3215	201.4	3241	180.1	3310	592.6	3310	412	3015	2.1	2943	1.9
G32	2000	4000	N/A	N/A	1136	6.8	1106	214.9	N/A	N/A	1338	92.7	1349	198.7	1360	180.1	1410	65.8	1410	330	1240	2.2	1226	1.7
G33	2000	4000	N/A	N/A	1106	6.6	1068	213.4	N/A	N/A	1302	89.3	1330	194.3	1342	180.1	1382	504.1	1382	349	1224	2.3	1208	1.7
G34	2000	4000	N/A	N/A	1118	5.8	1106	212.4	N/A	N/A	1314	95.6	1320	198.7	1350	180.1	1384	84.2	1384	302	1238	2.3	1220	1.6
G35	2000	11778	N/A	N/A	7358	9.4	6196	185.7	N/A	N/A	7495	95.2	6599	200.6	7624	180.1	7686	796.7	7686	1070	7245	1.9	7260	1.9

Table 6: Continued.

Instance	$\lvert\mathcal{V}\rvert$	$\lvert\mathcal{E}\rvert$	GW		MD		PI-GNN		Genetic		BQP		ECO-DQN		ANYCSP		MOH		LPI		ROS-vanilla		ROS	
			Obj. ↑	Time (s) ↓	Obj. ↑	Time (s) ↓	Obj. ↑	Time (s) ↓	Obj. ↑	Time (s) ↓	Obj. ↑	Time (s) ↓	Obj. ↑	Time (s) ↓	Obj. ↑	Time (s) ↓	Obj. ↑	Time (s) ↓	Obj. ↑	Time (s) ↓	Obj. ↑	Time (s) ↓	Obj. ↑	Time (s) ↓
G36	2000	11766	N/A	N/A	7336	10.1	6424	214.8	N/A	N/A	7490	95.3	6602	195.1	7628	180.1	7680	664.5	7680	5790	7235	2.4	7107	1.5
G37	2000	11785	N/A	N/A	7400	9.3	6224	185.3	N/A	N/A	7498	95.4	6555	204.1	7617	180.1	7691	652.8	7691	4082	7164	1.7	7141	1.5
G38	2000	11779	N/A	N/A	7343	8.6	6841	212.8	N/A	N/A	7507	100.6	6655	200.3	7629	180.1	7688	779.7	7688	614	7114	1.6	7173	1.8
G39	2000	11778	N/A	N/A	1998	9.2	1853	215.5	N/A	N/A	2196	94.4	1904	198.8	2354	180.1	2408	787.7	2408	347	2107	2.5	2165	1.7
G40	2000	11766	N/A	N/A	1971	9.0	1855	216.0	N/A	N/A	2169	97.3	2171	199.8	2320	180.1	2400	472.5	2400	314	2207	2.7	2128	2.5
G41	2000	11785	N/A	N/A	1969	9.1	1898	218.6	N/A	N/A	2183	105.8	1925	203.7	2346	180.1	2405	377.4	2405	286	2120	1.6	2139	2.2
G42	2000	11779	N/A	N/A	2075	9.5	1933	206.3	N/A	N/A	2255	95.5	2152	200.1	2416	180.1	2481	777.4	2481	328	2200	2.2	2235	2.4
G43	1000	9990	6340	1784.5	6380	5.0	6049	186.9	5976	914.4	6509	18.0	6585	44.3	6631	180.1	6660	1.2	6660	19	6539	2.7	6471	1.7
G44	1000	9990	6351	1486.7	6327	5.0	6099	190.8	6009	914.3	6463	18.5	6577	42.2	6632	180.1	6650	5.3	6650	20	6498	2.5	6472	1.7
G45	1000	9990	6355	1582.0	6329	4.9	6091	189.6	6006	921.5	6489	22.4	6581	41.3	6632	180.1	6654	6.9	6654	19	6528	2.4	6489	1.7
G46	1000	9990	6357	1612.8	6300	4.8	5594	188.6	5978	916.2	6485	18.4	6570	43.8	6631	180.1	6649	67.3	6649	21	6498	2.5	6499	2.5
G47	1000	9990	N/A	N/A	6369	4.7	6049	184.8	5948	912.4	6491	18.4	6575	46.8	6655	180.1	6657	43.3	6657	25	6497	2.5	6489	1.8
G48	3000	6000	N/A	N/A	5006	10.6	4958	191.4	N/A	N/A	6000	300.4	5879	881.2	5962	180.2	6000	0.0	6000	94	5640	3.2	5498	2.1
G49	3000	6000	N/A	N/A	5086	10.1	4938	192.0	N/A	N/A	6000	303.0	5879	871.5	5936	180.2	6000	0.0	6000	93	5580	3.1	5452	2.2
G50	3000	6000	N/A	N/A	5156	11.3	4948	192.3	N/A	N/A	5880	299.8	5807	876.7	5830	180.2	5880	532.1	5880	90	5656	3.2	5582	1.9
G51	1000	5909	N/A	N/A	3693	4.1	3293	188.5	3568	887.9	3759	17.7	3413	45.0	3821	180.2	3848	189.2	3848	145	3629	1.5	3677	1.7
G52	1000	5916	N/A	N/A	3695	4.7	3185	183.8	3575	897.7	3771	18.5	3441	41.9	3836	180.2	3851	209.7	3851	119	3526	1.3	3641	1.6
G53	1000	5914	N/A	N/A	3670	4.5	3029	170.6	3545	872.8	3752	18.0	3469	38.3	3807	180.2	3850	299.3	3850	182	3633	1.5	3658	1.6
G54	1000	5916	N/A	N/A	3682	4.4	3201	189.3	3548	880.1	3753	18.0	3485	44.6	3820	180.2	3852	190.4	3852	140	3653	1.6	3642	1.3
G55	5000	12498	N/A	N/A	9462	24.4	9110	201.5	N/A	N/A	9862	1142.1	N/A	N/A	10213	180.2	10299	1230.4	10299	6594	9819	2.1	9779	2.9
G56	5000	12498	N/A	N/A	3203	23.8	2939	201.8	N/A	N/A	3710	1147.6	N/A	N/A	3918	180.2	4016	990.4	4017	49445	3444	2	3475	2.5
G57	5000	10000	N/A	N/A	2770	17.3	2650	203.0	N/A	N/A	3310	1120.8	N/A	N/A	3404	180.2	3494	1528.3	3494	3494	3040	1.7	3078	2.5
G58	5000	29570	N/A	N/A	18452	29.2	17115	202.8	N/A	N/A	18813	1176.6	N/A	N/A	19152	180.2	19288	1522.3	19294	65737	17632	2.3	17574	1.8
G59	5000	29570	N/A	N/A	5099	31.6	4674	202.6	N/A	N/A	5490	1183.4	N/A	N/A	5952	180.2	6087	2498.8	6088	65112	5343	1.9	5407	4.7
G60	7000	17148	N/A	N/A	13004	34.8	11430	214.0	N/A	N/A	N/A	N/A	N/A	N/A	14096	180.2	14190	2945.4	14190	44802	13433	2	13402	2
G61	7000	17148	N/A	N/A	4592	36.0	4225	213.9	N/A	N/A	N/A	N/A	N/A	N/A	5710	180.2	5798	6603.3	5798	74373	5037	3.8	5011	2
G62	7000	14000	N/A	N/A	3922	26.1	3720	214.0	N/A	N/A	N/A	N/A	N/A	N/A	4732	180.2	4868	5568.6	4872	26537	4252	3.8	4294	2.8
G63	7000	41459	N/A	N/A	25938	45.1	22224	213.9	N/A	N/A	N/A	N/A	N/A	N/A	26884	180.2	27033	6492.1	27033	52726	24185	1.7	24270	1.5
G64	7000	41459	N/A	N/A	7283	43.7	6616	212.9	N/A	N/A	N/A	N/A	N/A	N/A	8514	180.4	8747	4011.1	8752	49158	7508	2.3	7657	3
G65	8000	16000	N/A	N/A	4520	32.5	4208	220.4	N/A	N/A	N/A	N/A	N/A	N/A	5392	180.1	5560	4709.5	5562	21737	4878	4.4	4826	2.5
G66	9000	18000	N/A	N/A	5100	37.3	4816	223.1	N/A	N/A	N/A	N/A	N/A	N/A	6172	159.6	6360	6061.9	6364	34062	5570	5.5	5580	3.3
G67	10000	20000	N/A	N/A	5592	43.4	5312	258.9	N/A	N/A	N/A	N/A	N/A	N/A	6772	146.5	6942	4214.3	6948	61556	6090	6.2	6010	1.9
G70	10000	9999	N/A	N/A	8551	54.3	8404	217.5	N/A	N/A	N/A	N/A	N/A	N/A	9300	180.2	9544	8732.4	9594	28820	9004	4.9	8916	3.4
G72	10000	20000	N/A	N/A	5638	44.2	5386	217.6	N/A	N/A	N/A	N/A	N/A	N/A	6826	180.2	6998	6586.6	7004	42542	6066	6.2	6102	3.9
G77	14000	28000	N/A	N/A	7934	66.0	7352	291.0	N/A	N/A	N/A	N/A	N/A	N/A	9694	180.2	9928	9863.6	9926	66662	8678	9	8740	8.1
G81	20000	40000	N/A	N/A	11226	130.8	10582	494.1	N/A	N/A	N/A	N/A	N/A	N/A	13684	180.2	14036	20422.0	14030	66691	12260	13.7	12332	9.3

Table 7: Complete results on Gset instances for Max-3-Cut.

Instance	$\|\mathcal{V}\|$	$\|\mathcal{E}\|$	MD		Genetic		BQP		ANYCSP		MOH		ROS-vanilla		ROS	
			Obj. ↑	Time (s) ↓	Obj. ↑	Time (s) ↓	Obj. ↑	Time (s) ↓	Obj. ↑	Time (s) ↓	Obj. ↑	Time (s) ↓	Obj. ↑	Time (s) ↓	Obj. ↑	Time (s) ↓
G1	800	19176	14735	9.6	14075	595.3	14880	16.5	15115	180.1	15165	557.3	14949	2.8	14961	1.9
G2	800	19176	14787	8.4	14035	595.3	14845	17.0	15088	180.1	15172	333.3	15033	2.8	14932	2.3
G3	800	19176	14663	6.5	14105	588.6	14872	17.0	15111	180.1	15173	269.6	15016	2.9	14914	1.9
G4	800	19176	14716	6.9	14055	588.7	14886	17.1	15115	180.1	15184	300.6	14984	3.3	14961	1.9
G5	800	19176	14681	8.1	14104	591.9	14847	17.3	15092	180.1	15193	98.2	15006	3.2	14962	2.9
G6	800	19176	2161	7.8	1504	604.4	2302	25.0	1164	180.1	2632	307.3	2436	2.8	2361	1.8
G7	800	19176	2017	8.9	1260	589.9	2081	16.6	932	180.1	2409	381.0	2188	2.1	2188	2.4
G8	800	19176	1938	7.7	1252	589.7	2096	19.3	1007	180.1	2428	456.5	2237	2.8	2171	2.1
G9	800	19176	2031	8.2	1326	604.4	2099	16.5	1164	180.1	2478	282.0	2246	2.8	2185	2.2
G10	800	19176	1961	7.5	1266	593.3	2055	18.2	919	180.1	2407	569.3	2201	2.9	2181	2.3
G11	800	1600	553	4.0	414	554.5	624	16.4	650	180.1	669	143.8	616	2	591	1.4
G12	800	1600	530	4.4	388	543.6	608	17.4	633	180.1	660	100.7	604	2	582	1.5
G13	800	1600	558	4.0	425	550.8	638	18.9	663	180.1	686	459.4	617	2	629	1.4
G14	800	4694	3844	5.0	3679	571.1	3900	16.9	3973	180.1	4012	88.2	3914	2.8	3892	2.1
G15	800	4661	3815	4.8	3625	567.6	3885	17.3	3975	180.1	3984	80.3	3817	1.9	3838	2
G16	800	4672	3825	5.3	3642	561.5	3896	18.2	3945	180.1	3991	1.3	3843	2.3	3845	1.6
G17	800	4667	3815	5.3	3640	558.7	3886	20.2	3955	180.1	3983	7.8	3841	2.4	3852	1.6
G18	800	4694	992	4.5	704	584.0	1083	18.7	999	180.1	1207	0.3	1094	2.2	1067	1.7
G19	800	4661	869	4.4	595	584.2	962	17.0	915	180.1	1081	0.2	972	2.1	967	1.7
G20	800	4672	928	4.5	589	576.8	977	17.0	861	180.1	1122	13.3	1006	2.2	993	1.8
G21	800	4667	936	4.9	612	576.3	984	17.5	895	180.1	1109	55.8	1011	2.2	975	1.5
G22	2000	19990	16402	15.2	N/A	N/A	16599	135.5	17098	180.1	17167	28.5	16790	3.3	16601	2.2
G23	2000	19990	16422	15.0	N/A	N/A	16626	135.6	17049	180.1	17168	45.1	16819	3.9	16702	2.1
G24	2000	19990	16452	16.1	N/A	N/A	16591	137.7	17042	180.1	17162	16.3	16801	3.6	16754	3
G25	2000	19990	16407	16.2	N/A	N/A	16661	141.8	17085	180.1	17163	64.8	16795	2.1	16673	1.8
G26	2000	19990	16422	15.3	N/A	N/A	16608	136.3	17014	180.1	17154	44.8	16758	3.1	16665	2
G27	2000	19990	3250	16.4	N/A	N/A	3475	134.3	2846	180.1	4020	53.2	3517	1.7	3532	2
G28	2000	19990	3198	16.1	N/A	N/A	3433	136.4	2778	180.1	3973	38.9	3507	3	3414	2.1
G29	2000	19990	3324	16.0	N/A	N/A	3582	136.2	3035	180.1	4106	68.2	3634	3.4	3596	2
G30	2000	19990	3320	16.2	N/A	N/A	3578	133.6	3032	180.1	4119	150.4	3656	3.1	3654	3.4
G31	2000	19990	3243	17.0	N/A	N/A	3439	131.0	2881	180.1	4003	124.7	3596	3	3525	2.5
G32	2000	4000	1342	11.1	N/A	N/A	1545	129.3	1590	180.1	1653	160.1	1488	2.5	1482	1.7
G33	2000	4000	1284	10.7	N/A	N/A	1517	126.2	1550	180.1	1625	62.6	1449	2.5	1454	2
G34	2000	4000	1292	10.9	N/A	N/A	1499	126.0	1525	180.1	1607	88.9	1418	2.4	1435	1.7
G35	2000	11778	9644	14.2	N/A	N/A	9816	138.1	9968	180.1	10046	66.2	9225	2	9536	1.7

Table 7: Continued.

Instance	$\lvert\mathcal{V}\rvert$	$\lvert\mathcal{E}\rvert$	MD		Genetic		BQP		ANYCSP		MOH		ROS-vanilla		ROS	
			Obj. ↑	Time (s) ↓	Obj. ↑	Time (s) ↓	Obj. ↑	Time (s) ↓	Obj. ↑	Time (s) ↓	Obj. ↑	Time (s) ↓	Obj. ↑	Time (s) ↓		
G36	2000	11766	9600	13.6	N/A	N/A	9786	138.6	9972	180.1	10039	74.3	9372	2.1	9581	2.3
G37	2000	11785	9632	14.9	N/A	N/A	9821	139.2	9983	180.1	10052	3.4	8893	1.4	9422	1.5
G38	2000	11779	9629	14.0	N/A	N/A	9775	142.3	9980	180.1	10040	116.6	9489	2.5	9370	1.5
G39	2000	11778	2368	13.4	N/A	N/A	2600	132.8	2497	180.1	2903	9.0	2621	2.5	2557	2.2
G40	2000	11766	2315	13.3	N/A	N/A	2568	131.2	2428	8.6	2870	82.8	2474	2	2524	2.4
G41	2000	11785	2386	12.7	N/A	N/A	2606	129.9	2416	8.4	2887	87.7	2521	3.2	2584	2.5
G42	2000	11779	2490	13.1	N/A	N/A	2682	129.2	2685	32.8	2980	2.5	2638	2.7	2613	2.2
G43	1000	9990	8214	8.1	7624	926.7	8329	29.9	8531	180.1	8573	380.3	8414	2.6	8349	2.3
G44	1000	9990	8187	7.0	7617	919.0	8326	27.7	8515	180.1	8571	616.8	8369	2.6	8311	1.7
G45	1000	9990	8226	7.7	7602	926.7	8296	34.2	8530	180.1	8566	186.2	8397	2.9	8342	1.8
G46	1000	9990	8229	7.5	7635	918.7	8312	27.8	8501	180.1	8568	215.3	8409	2.6	8339	1.7
G47	1000	9990	8211	7.2	7619	928.0	8322	27.3	8513	180.2	8572	239.4	8386	2.6	8357	2.2
G48	3000	6000	5806	14.7	N/A	N/A	5998	394.8	5985	180.2	6000	0.4	5954	2.8	5912	2
G49	3000	6000	5794	14.4	N/A	N/A	5998	404.0	5974	180.2	6000	0.9	5938	2.8	5914	1.8
G50	3000	6000	5823	14.5	N/A	N/A	6000	427.1	5989	180.2	6000	119.2	5938	2.9	5918	1.8
G51	1000	5909	4805	6.6	4582	889.5	4922	28.6	4990	180.2	5037	47.9	4814	2.4	4820	1.7
G52	1000	5916	4849	6.4	4571	908.1	4910	27.8	5002	180.2	5040	0.7	4796	1.9	4866	1.9
G53	1000	5914	4845	6.8	4568	898.6	4920	27.6	5005	180.2	5039	223.9	4846	2.6	4808	1.6
G54	1000	5916	4836	6.4	4562	911.7	4921	30.1	4998	180.2	5036	134.0	4833	2.2	4785	1.4
G55	5000	12498	11612	37.9	N/A	N/A	12042	1506.0	12355	180.2	12429	383.1	12010	2.1	11965	2.6
G56	5000	12498	3716	38.5	N/A	N/A	4205	1341.5	4408	180.2	4752	569.2	4085	3.3	4037	2.1
G57	5000	10000	3246	33.0	N/A	N/A	3817	1317.2	3913	180.2	4083	535.6	3597	3.3	3595	2.8
G58	5000	29570	24099	47.1	N/A	N/A	24603	1468.3	25025	180.2	25195	576.0	22748	2.1	23274	1.9
G59	5000	29570	6057	46.3	N/A	N/A	6631	1377.1	6178	180.2	7262	27.5	6133	1.7	6448	3.5
G60	7000	17148	15993	58.5	N/A	N/A	N/A	N/A	16974	180.2	17076	683.0	16467	2.6	16398	2.3
G61	7000	17148	5374	57.7	N/A	N/A	N/A	N/A	6426	180.2	6853	503.1	5881	2.5	5861	3.6
G62	7000	14000	4497	49.7	N/A	N/A	N/A	N/A	5444	180.2	5685	242.4	4983	3.4	5086	2.7
G63	7000	41459	33861	73.4	N/A	N/A	N/A	N/A	35070	180.2	35322	658.5	32868	4	31926	1.9
G64	7000	41459	8773	73.4	N/A	N/A	N/A	N/A	8557	180.4	10443	186.9	8911	2.8	9171	2.5
G65	8000	16000	5212	59.6	N/A	N/A	N/A	N/A	6232	180.1	6490	324.7	5735	3.5	5775	2.6
G66	9000	18000	5948	69.0	N/A	N/A	N/A	N/A	7129	159.6	7416	542.5	6501	5.4	6610	3.9
G67	10000	20000	6545	79.0	N/A	N/A	N/A	N/A	7827	146.5	8086	756.7	7001	3.5	7259	4.1
G70	10000	9999	9718	74.8	N/A	N/A	N/A	N/A	9848	180.2	9999	7.8	9982	4.2	9971	2.5
G72	10000	20000	6612	79.2	N/A	N/A	N/A	N/A	7893	180.2	8192	271.2	7210	5.1	7297	3.5
G77	14000	28000	9294	142.3	N/A	N/A	N/A	N/A	11128	180.2	11578	154.9	10191	8.6	10329	8.5
G81	20000	40000	13098	241.1	N/A	N/A	N/A	N/A	15658	180.2	16321	331.2	14418	20.2	14464	9.7

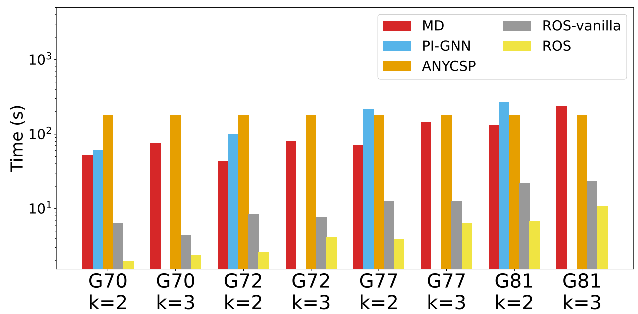

(a) Weighted Gset with perturbation ratio $[0.9, 1.1]$

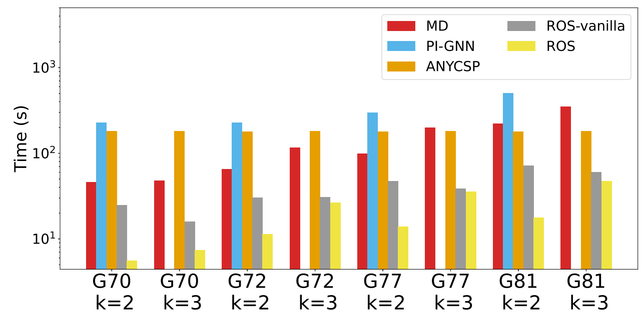

(b) Weighted Gset with perturbation ratio $[0, 100]$

Figure 4: The computational time comparison of Max-k-Cut problems.

Table 8: Cut value comparison of Max-k-Cut problems on weighted Gset instances with perturbation ratio $[0.9, 1.1]$.

Methods	G70 (N=10,000)		G72 (N=10,000)		G77 (N=14,000)		G81 (N=20,000)	
	$k=2$	$k=3$	$k=2$	$k=3$	$k=2$	$k=3$	$k=2$	$k=3$
MD	8594.38	9709.56	5647.28	6585.04	8051.81	9337.31	11326.30	13179.33
PI-GNN	8422.79	–	5309.65	–	7470.89	–	10416.44	–
ANYCSP	5198.87	5375.92	-15.57	-25.33	81.76	114.36	33.49	-4.25
ROS-vanilla	9177.21	9991.95	6542.78	7733.87	9265.65	10944.35	13132.52	15456.28
ROS	8941.80	9970.72	6165.62	7366.54	8737.59	10359.25	12325.85	14570.04

E. The Results on Weighted Gset Instances

The computational time on weighted Gset with perturbation ratio of $[0.9, 1.1]$ and $[0, 100]$ are shown in Fig. 4a and Fig. 4b respectively. The cut values are shown in Table 8 and Table 9 respectively.

F. Ablation Study

F.1. Model Ablation

We conducted additional ablation studies to clarify the contributions of different modules.

Effect of Neural Networks: We consider two cases: (i) replace GNNs by multi-layer perceptrons (denoted by `ROS-MLP`) in our ROS framework and (ii) solve the relaxation via mirror descent (denoted by `MD`). Experiments on the Gset dataset show that `ROS` consistently outperforms `ROS-MLP` and `MD`, highlighting the benefits of using GNNs for the relaxation step.

Effect of Random Sampling: We compared `ROS` with `PI-GNN`, which employs heuristic rounding instead of our random sampling algorithm. Results indicate that `ROS` generally outperforms `PI-GNN`, demonstrating the importance of the sampling procedure.

These comparisons, detailed in Tables 10 and 11, confirm that both the GNN-based optimization and the random sampling algorithm contribute significantly to the overall performance.

F.2. Sample Effect Ablation

We investigated the effect of the number of sampling iterations and report the results in Tables 12, 13, 14, and 15.

Cut Value (Table 12, Table 14): The cut values stabilize after approximately 5 sampling iterations, demonstrating strong performance without requiring extensive sampling.

Sampling Time (Table 13, Table 15): The time spent on sampling remains negligible compared to the total computational

Table 9: Cut value comparison of Max-k-Cut problems on weighted Gset instances with perturbation ratio $[0, 100]$.

Methods	G70 (N=10,000)		G72 (N=10,000)		G77 (N=14,000)		G81 (N=20,000)	
	$k=2$	$k=3$	$k=2$	$k=3$	$k=2$	$k=3$	$k=2$	$k=3$
MD	456581.30	497167.48	338533.07	392908.80	482413.19	558264.21	682809.47	790089.41
PI-GNN	442650.59	–	312802.48	–	442354.44	–	623256.74	–
ANYCSP	467696.98	491654.75	-1903.50	-2498.86	9712.13	10130.89	2842.64	2845.46
ROS-vanilla	472067.14	498273.60	367795.62	421189.97	524010.92	597597.50	742432.41	846395.85
ROS	470268.97	498269.90	362910.89	415905.88	515991.31	590312.40	731468.67	835424.19

Table 10: Cut values returned by each method on Gset.

Methods	G70		G72		G77		G81	
	$k=2$	$k=3$	$k=2$	$k=3$	$k=2$	$k=3$	$k=2$	$k=3$
ROS-MLP	8867	9943	6052	6854	8287	9302	12238	12298
PI-GNN	8956	–	4544	–	6406	–	8970	–
MD	8551	9728	5638	6612	7934	9294	11226	13098
ROS	8916	9971	6102	7297	8740	10329	12332	14464

time, even with an increased number of samples.

These results highlight the efficiency of our sampling method, achieving stable and robust performance with little computational cost.

Table 11: Computational time for each method on Gset.

Methods	G70		G72		G77		G81	
	$k=2$	$k=3$	$k=2$	$k=3$	$k=2$	$k=3$	$k=2$	$k=3$
ROS-MLP	3.49	3.71	3.93	4.06	8.39	9.29	11.98	16.97
PI-GNN	34.50	–	253.00	–	349.40	–	557.70	–
MD	54.30	74.80	44.20	79.20	66.00	142.30	130.80	241.10
ROS	3.40	2.50	3.90	3.50	8.10	8.50	9.30	9.70

Table 12: Cut value results corresponding to the times of sample T on Gset.

T	G70		G72		G77		G81	
	$k=2$	$k=3$	$k=2$	$k=3$	$k=2$	$k=3$	$k=2$	$k=3$
0	8912.62	9968.11	6099.88	7304.45	8736.58	10323.61	12328.83	14458.09
1	8911	9968	6100	7305	8736	10321	12328	14460
5	8915	9969	6102	7304	8740	10326	12332	14462
10	8915	9971	6102	7305	8740	10324	12332	14459
25	8915	9971	6102	7307	8740	10326	12332	14460
50	8915	9971	6102	7307	8740	10327	12332	14461
100	8916	9971	6102	7308	8740	10327	12332	14462

Table 13: Sampling time results corresponding to the times of sample T on Gset.

T	G70		G72		G77		G81	
	$k=2$	$k=3$	$k=2$	$k=3$	$k=2$	$k=3$	$k=2$	$k=3$
1	0.0011	0.0006	0.0011	0.0006	0.0020	0.0010	0.0039	0.0020
5	0.0030	0.0029	0.0029	0.0030	0.0053	0.0053	0.0099	0.0098
10	0.0058	0.0059	0.0058	0.0058	0.0104	0.0104	0.0196	0.0196
25	0.0144	0.0145	0.0145	0.0145	0.0259	0.0260	0.0489	0.0489
50	0.0289	0.0289	0.0288	0.0289	0.0517	0.0518	0.0975	0.0977
100	0.0577	0.0577	0.0576	0.0578	0.1033	0.1037	0.1949	0.1953

Table 14: Cut value results corresponding to the times of sample T on random regular graphs.

T	$n=100$		$n=1,000$		$n=10,000$	
	$k=2$	$k=3$	$k=2$	$k=3$	$k=2$	$k=3$
0	126.71	244.77	1291.86	2408.71	12856.53	24102.22
1	127	245	1293	2408	12856	24103
5	127	245	1293	2410	12863	24103
10	127	245	1293	2410	12862	24103
25	127	245	1293	2410	12864	24103
50	127	245	1293	2410	12864	24103
100	127	245	1293	2410	12864	24103

Table 15: Sampling time results corresponding to the times of sample T on random regular graphs.

T	$n = 100$		$n = 1,000$		$n = 10,000$	
	$k = 2$	$k = 3$	$k = 2$	$k = 3$	$k = 2$	$k = 3$
1	0.0001	0.0001	0.0001	0.0001	0.0006	0.0006
5	0.0006	0.0006	0.0007	0.0007	0.0030	0.0030
10	0.0011	0.0011	0.0014	0.0013	0.0059	0.0059
25	0.0026	0.0026	0.0033	0.0031	0.0145	0.0145
50	0.0052	0.0052	0.0065	0.0060	0.0289	0.0289
100	0.0103	0.0103	0.0128	0.0122	0.0577	0.0578